The interaction landscape between transcription factors and the nucleosome

Fangjie Zhu[1], Lucas Fanung[2], Eevi Kaasinen[1], Biswajyoti Sahu[1], Yimeng Yin[1], Bei Wei[1], Svetlana Dodonova[2], Patrick Cramer[2,3] and Jussi Taipale[1,4,*]

[1]Division of Functional Genomics and Systems Biology, Department of Medical Biochemistry and Biophysics, Karolinska Institutet, Scheeles väg 2, SE 171 77 Stockholm, Sweden.

[2]Max Planck Institute for Biophysical Chemistry, Department of Molecular Biology, Am Fassberg 11, D-37077 Göttingen, Germany.

[3]Center for Innovative Medicine and Science for Life Laboratory, Department of Biosciences and Nutrition, Karolinska Institutet, Hälsovägen 7, SE 141 83 Stockholm, Sweden.

[4]Genome-Scale Biology Program, Post Office Box 63, FI-00014 University of Helsinki, Helsinki, Finland.

**To whom correspondence should be addressed. E-mail: jussi.taipale@ki.se*

Nucleosomes cover most of the genome and are thought to be displaced by transcription factors (TFs) in regions that direct gene expression. However, the modes of interaction between TFs and nucleosomal DNA remain largely unknown. Here, we use nucleosome consecutive affinity-purification systematic evolution of ligands by exponential enrichment (NCAP-SELEX) to systematically explore interactions between the nucleosome and 220 TFs representing diverse structural families. Consistently with earlier observations, we find that the vast majority of TFs have less access to nucleosomal DNA than to free DNA. The motifs recovered from TFs bound to nucleosomal and free DNA are generally similar; however, steric hindrance and scaffolding by the nucleosome result in specific positioning and orientation of the motifs. Many TFs preferentially bind close to the end of nucleosomal DNA, or to periodic positions at its solvent-exposed side. TFs often also bind nucleosomal DNA in a particular orientation, because the nucleosome breaks the local rotational symmetry of DNA. Some TFs also specifically interact with DNA located at the dyad position where only one DNA gyre is wound, whereas other TFs prefer sites spanning two DNA gyres and bind specifically to each of them. Our work reveals striking differences in TF binding to free and nucleosomal DNA, and uncovers a rich interaction landscape between the TFs and the nucleosome.

Simple prokaryotic organisms such as *E.coli* have relatively small genomes, which are often organized into a circular chromosome consisting of a single DNA molecule. Their genes are regulated by TFs that directly bind to the free DNA molecule and influence transcriptional activity. Eukaryotic genomes, however, are much larger, and need to be packaged more efficiently inside the nucleus. The packaging is accomplished by a specific class of basic proteins, the histones, which exist as an octameric complex and bind to the DNA backbone, forming nucleosomes[1-4]. In a canonical nucleosome, a 147 bp segment of DNA is wrapped around the histone octamer in a left-handed, superhelical arrangement for a total of 1.65 turns, with the DNA helix entering and exiting the nucleosome from the same side of the histone octamer. The two DNA gyres are paralleling each other except at the position located between the entering and the exiting DNA, where a dyad region of ~15 bp contains only a single DNA gyre. The nucleosome is 2-fold pseudo-symmetric with respect to a dyad axis at the center of the dyad region. Approximately 70% of eukaryotic DNA is packaged into nucleosomes, separated from each other by free DNA linker sequences of 10–80 bp[5-7].

The nucleosome presents a significant barrier for binding of other proteins such as RNA polymerases to DNA[8-14]. As a consequence, the presence of nucleosomes can have a negative effect on gene expression. Similarly, most TFs are thought to be unable to bind to nucleosomal DNA, and TF binding sites in the genome are usually depleted of nucleosomes[15-17]. However, it is thought that a specific class of TFs, the pioneer factors, can access nucleosomal DNA, and assist the binding of other TFs to nearby sites[18-22]. Many TFs that have essential roles in development and cell reprogramming are pioneer factors[23,24]. Two different mechanisms have been suggested to be responsible for the pioneering activity: mimicking the linker histones[25] and/or targeting a partial TF motif that is accessible on nucleosomal DNA[26].

Nucleosomes can also indirectly induce cooperativity between multiple TF binding events[27-31]. This cooperation can occur in the absence of direct TF-TF interactions[32], allowing multiple weak binding events to dissociate nucleosomes, resulting in a preferred range of spacings between the two TF binding sites[33]. Consistently, in higher eukaryotes, most occupied TF binding sites are clustered to short genomic regions[34-37].

Despite the importance of the nucleosome in both chromatin organization and transcriptional control, the effect of nucleosomes on TF binding has not been systematically characterized. This is in part because the sites bound by both a TF and a nucleosome are difficult to identify in cells, as the methods to map cellular TF binding locations are imprecise. Furthermore, TF-nucleosome complexes that activate chromatin remodeling in cells are expected to be unstable, and thus hard to capture experimentally. In our recent work, we found that scaffolding by DNA results in a large number of interactions between transcription factors[38]. Given that the DNA scaffold is bent and partially blocked by the nucleosome, it is likely that nucleosome occupancy will also have a major effect on TF-DNA binding.

RESULTS

Nucleosome CAP-SELEX

To determine the effect of nucleosome on TF-DNA binding, we adapted our previous Consecutive Affinity-Purification SELEX (CAP-SELEX) method[38] to include nucleosome reconstitution. We name this approach Nucleosome CAP-SELEX (NCAP-SELEX). We designed two types of SELEX ligands, a 147 bp (lig147) and a 200 bp (lig200) ligand, containing 101 bp and 154 bp randomized regions, respectively. In the NCAP-SELEX assay (**Fig. 1a**), recombinant histone octamers containing tagged H2A proteins (**Extended Data Fig. 1a, b**) are first loaded onto the DNA ligands (**Extended Data Fig. 1c, d**) in 384-well microplates by decreasing the salt concentration in a stepwise fashion (see **Methods** and Dyer *et al*.[39]). Subsequently, the nucleosomes are purified using magnetic beads. Eluted nucleosomes are incubated with TFs having an orthogonal tag, and the TF-bound species are subsequently pulled-down. The bound DNA is then amplified using PCR, and the entire process is repeated for a total of five times. To determine whether the TF binding induces dissociation of nucleosomes, the nucleosomes are recaptured after the final cycle (**Fig. 1a**). Both the nucleosome-bound and unbound DNA of the final cycle, as well as input DNA and DNA from the earlier cycles are then sequenced using a massively parallel sequencer.

To determine the effect of nucleosomes on TF binding, the ligand sequences were analyzed computationally using motif matching, *de novo* motif discovery and mutual information pipelines as illustrated in **Extended Data Fig. 1e**. In most analyses, we estimate TF signals using an approach that is based on the mutual-information (MI) between 3-mer distributions at two non-overlapping positions of the ligand (**Fig. 1b**). The underlying rationale is that if a binding event contacts two positions of a SELEX ligand at the same time, the 3-mer distributions at these two positions would be correlated in the enriched library, with the joint distribution favoring the 3-mer combinations that form the high-affinity sites. This biased joint distribution would then be detected as an increase in MI between the positions. Such an approach has multiple advantages: it operates without previous knowledge of TF specificities, enables facile comparison of selectivity between different TFs, and pinpoints the positions where DNA interacts with the TFs.

For the library enriched by each TF, we calculated MI between all pairwise combinations of positions, and represented the results as a 2D heatmap (**Fig. 1b**). In the heatmap showing MI from all 3-mer pairs (total MI; **Fig. 1b**, right), stripes with ~ 10 bp spacing are visible in addition to the TF signals. These stripes reflect the nucleosome signal, as histones contact DNA at ~ 10 bp intervals[40-43]. To focus more on the TF signals, we further developed a measure that considers only the MI between the ten most enriched non-overlapping 3-mer pairs (E-MI; **Fig. 1b**, left). As TFs rarely bind or cooperate across a large span of DNA, their signals are usually located at the diagonal of the 2D E-MI map. Therefore, the E-MI diagonal (**Fig. 1b**, bottom left) captures most of the footprints of TFs on the ligands, and corresponds well with the distribution of matches to the TFs' motifs (**Fig. 1b**, bottom right).

We performed NCAP-SELEX using 413 human TF extended DNA binding domains (eDBDs) (details are given in **Supplementary Table 1** and **Methods**). The selected TFs

119 covered 28% of the high-confidence TFs reported by Vaquerizas *et al.*[44]. Among the tested
120 TFs, 220 eDBDs were successful (**Fig. 1c;** see **Methods** for details**)**.

121 **Nucleosome inhibits TF binding**

122 We next analyzed the effect of nucleosome on TF binding by clustering the E-MI
123 diagonal signals from the lig200. The result reveals that the binding of almost all TFs to DNA
124 is inhibited or spatially restricted by the presence of a nucleosome (**Fig. 2a**). The lig200 can
125 accommodate only one nucleosome, but allows multiple positions for it (**Fig. 2a**, schematic at
126 the center). The nucleosome occupancy is thus expected to increase towards the center of the
127 lig200. The penetration of the E-MI diagonal signal into the center, in turn, reflects the ability
128 of each TF to bind to nucleosomal DNA. Analysis of this data revealed that TFs from the
129 same family tend to cluster together based on the E-MI diagonal (**Fig. 2a**; SOX TFs indicated
130 as an example). However, the extent of the penetration varied strongly between the TFs (**Fig.**
131 **2b**). For example, SREBF1 and 2, and RFX3 (**Fig. 2c**, left) only show E-MI signal at the
132 extreme ends of the ligand, suggesting that they have weak affinity towards nucleosomal
133 DNA relative to free DNA. In contrast, TFs such as VSX1, ARX, and SOX12 display
134 stronger signal near the center (**Fig. 2c**, right), and are thus more capable of binding to the
135 nucleosome-occupied regions.

136 **TFs can bind sequences located on both nucleosomal DNA gyres**

137 For lig200 libraries, we next analyzed the entire 2D E-MI signals for individual TFs.
138 This analysis resulted in identification of a specific binding mode for T-box TFs on
139 nucleosomal DNA. Binding of brachyury (T) to nucleosomal DNA resulted in two prominent
140 E-MI signals (**Fig. 3a**, the heatmap). One was located at the E-MI diagonal, i.e. observed
141 between adjacent 3-mers, whereas the other resulted from 3-mers located ~ 80 bp from each
142 other. The first signal is due to the binding of T to nucleosomal DNA using motifs similar to
143 those found on free DNA (**Fig. 3a**, Mode 1). The second is associated with an approximately
144 80-bp-long motif (**Fig. 3a**, Mode 2), indicating a dimeric binding spanning the two gyres of
145 the nucleosomal DNA (**Fig. 3b**). We next compared the bound and unbound libraries of the
146 last cycle, and found that the signal for Mode 2 is stronger on the ligands that remained
147 bound to the nucleosome (**Fig. 3c**), indicating that the gyre-spanning binding stabilizes
148 mononucleosomes against dissociation. The Mode 2 binding is also observed for another T-
149 box factor, TBX2, and is not detected on free DNA (**Extended Data Fig. 2a, b**).

150 Interestingly, the scaffolding effect of the nucleosome also leads to TF binding modes
151 that contact nucleosomal DNA at positions spaced by approximately 40 bp (e.g. TBX2 and
152 ETV, as shown in **Extended Data Fig. 2b, c**). This effect is position-specific, with one
153 binding event being observed near the dyad, and the other(s) on the opposite side of the
154 nucleosome, with the two contacts separated by ~180°. As the individual TFs are located far
155 from each other in this binding mode, the binding pattern suggests that the nucleosome may
156 have two allosteric states or may form a higher order complex with these TFs.

157 Taken together, these results reveal that some TFs can interact with both DNA gyres
158 on the nucleosome, and suggest that nucleosome can generate novel composite TF-binding

159 sites on DNA by promoting spatial proximity of DNA sites that are located more distally on
160 free DNA.

161 **Nucleosome context breaks the rotational symmetry of DNA**

162 As DNA is double-stranded, TFs can bind to it in two different orientations. For TFs
163 that bind non-palindromic sites, their binding orientation can be determined from the bound
164 sequences. In analysis of motif matches on lig200, we noted that some TFs' motifs displayed
165 a bias of matches in one orientation at the 5' end, and in the other orientation at the 3' end of
166 the ligand. That is, these TFs have a preferred orientation relative to the nucleosome. We
167 systematically examined this asymmetric effect between binding orientations by comparing
168 the strand-wise distributions of top 8-mers (**Fig. 3d**, **Extended Data Fig. 3a,** see also
169 **Methods** for details).

170 Both the extent of the orientational asymmetry and the associated p-value (**Fig. 3d**)
171 revealed that many ETS factors displayed strong orientational preferences. ELF2 is shown in
172 **Fig. 3e** as an example; its motif distributions (**Fig. 3e**, upper panel) and top 8-mer
173 distributions (**Extended Data Fig. 3b**) display strong orientational preference. CREB factors
174 also show considerable orientational preference towards the nucleosome in NCAP-SELEX
175 (**Extended Data Fig. 3c**). The orientational asymmetry induced by the nucleosome can be
176 explained by the fact that DNA is rotationally pseudosymmetric, and this symmetry is broken
177 by the presence of the nucleosome (**Extended Data Fig. 3d**), leading to a different local
178 environment for a TF bound at the same position of DNA in opposite orientations (**Fig. 3e**,
179 red and yellow ovals). Depending on its orientation, a particular side of a TF will be in
180 proximity with either the second gyre of nucleosomal DNA, or the histone proteins.

181 The distributions of motif matches in the two strands were symmetric with regard to
182 the dyad position of the nucleosome. This, in turn, is a consequence of the pseudo 2-fold
183 symmetry of the nucleosome; two binding sites in different orientations will share an
184 identical configuration when they locate at opposite sides of the dyad, and have an equal
185 distance to the dyad (**Fig. 3e**, models in the lower panel).

186 To determine whether the directional binding of TFs to a nucleosome is also observed
187 *in vivo*, we performed MNase digestion followed by paired-end sequencing for the human
188 colorectal cancer cell line LoVo. We then visualized the distribution of MNase fragments
189 around directional ELF2 motif matches within ELF2 ChIP-seq peaks from Yan et al.[37] (**Fig.**
190 **3f**). As described previously[45], this visualization reveals nucleosomes near the TF sites due to
191 enrichment of fragments whose size corresponds to a single nucleosome. The footprint of the
192 TF is also seen as a V-shaped line having lower signal intensity (arrowheads in **Fig. 3f**). This
193 analysis shows that both the nucleosome distribution and the TF footprint size are
194 asymmetric with respect to the ELF2 sites. For the specified motif direction, the footprint of
195 ELF2 is more distinct downstream of the nucleosome than upstream of it. This implies a
196 more stable binding of ELF2 downstream of the nucleosome, which is in accordance with the
197 motif match analysis from the ELF2 NCAP-SELEX data (**Fig. 3e**). The MNase analysis also
198 indicated that nucleosome occupancy is lower upstream than that downstream of ELF2 sites.
199 This pattern suggests that the more stable binding of ELF2 downstream of the nucleosome

200 displaces the nucleosome or pushes it upstream. Similar to ELF2, the binding profile of ELF1
201 is also asymmetric with regard to nucleosome both in SELEX and *in vivo* (**Extended Data**
202 **Fig. 3e**).

203 **Nucleosome induces positional preference to TF binding**

204 We next analyzed the positional preference of TF binding on nucleosomal DNA using
205 the short lig147 ligand. Because its 147-bp length exactly matches the preferred length of
206 nucleosomal DNA, the nucleosome is expected to be uniquely positioned at the center of
207 lig147. Therefore, the relative positioning of the TFs with respect to the nucleosome can be
208 inferred at a higher resolution than using lig200. To determine the positional preference, we
209 first checked whether TFs' motifs on nucleosomal DNA are different from their motifs on
210 free DNA. For this purpose, we compared the most enriched 9-mer sequences for each TF,
211 between its lig147 libraries enriched either in the presence and absence of the nucleosome
212 **(Extended Data Fig. 4a)**. The result shows that most TFs bind to similar 9-mers under both
213 conditions, suggesting that TFs are binding nucleosomal DNA without significant specificity
214 changes. However, consistent with earlier observations[26], we also found few cases where the
215 binding specificities of the TFs were detectably different on nucleosomal DNA (**Extended**
216 **Data Fig. 4b**).

217 Analysis of TF binding to lig147 revealed several types of positional preference (**Fig.**
218 **4a**), which we classified into three major classes (**Fig. 4a**): (1) End binders; these TFs tend to
219 prefer positions towards the end of the ligand. All tested bZIP factors belong to this class
220 (**Fig. 4b**), e.g., CEBPB (**Fig. 4c, Extended Data Fig. 5a**). This preference might be
221 explained by the "breathing", i.e. the spontaneous partial detachment of nucleosomal
222 DNA[1,46,47], which occurs more frequently towards the entry and exit of nucleosomal DNA
223 (**Fig. 4d**). (2) Periodic binders; these TFs tend to bind periodic positions on nucleosomal
224 DNA. This periodicity is likely induced by the contacts of histones to DNA at 10-bp
225 intervals. (3) Dyad binders; these TFs prefer to bind nucleosomal DNA near the dyad
226 position. In addition to these three classes, we also identified a "mixed" class (**Fig. 4a**) where
227 TFs show E-MI diagonal characteristics of both the end binder and the periodic binder class.
228 TFs behaved consistently for lig147 and lig200 according to the binder classification
229 (**Extended Data Fig. 5b**). Compared to the end binders, the periodic binders and dyad
230 binders displayed deeper penetration of E-MI signals into the center of the ligands (**Extended**
231 **Data Fig. 5b**); they are thus more capable to bind nucleosomal DNA.

232 **Binding at the outward-facing side of the DNA helix**

233 Half of the circumference of nucleosomal DNA is in close proximity of the histones.
234 As DNA is helical, equivalent positions that could be accessible to TFs are thus located at
235 ~10 bp intervals. Accordingly, we found that many TFs prefer to bind to positions located
236 ~10 bp apart on nucleosomal DNA (**Fig. 4a**, periodic binders). We studied this effect using
237 the lig147 libraries. By applying a Fast Fourier Transform (FFT) to the E-MI diagonals, we
238 obtained the strength and phase of the ~10 bp periodicity for the TFs (**Fig. 5a**). The result
239 shows that the overall periodicity of E-MI is stronger for the NCAP-SELEX library
240 compared to the free-DNA HT-SELEX library (**Fig. 5a**, bottom). Due to the binding

241 specificity of nucleosome, an increased periodicity was also observed with the counts of
242 dinucleotides (e.g. TA) along the ligand (**Extended Data Fig. 6a**). TA-enriched positions on
243 nucleosomal DNA correspond to positions where histones contact DNA[4,42], which are also
244 positions where the DNA major groove is facing towards the solvent. The periodicity of TA
245 for all experiments had a similar phase (**Extended Data Fig. 6a**), suggesting that in NCAP-
246 SELEX, the nucleosomes reconstituted for all TFs shared a similar rotational position on the
247 DNA ligand. In contrast, the phase of the E-MI periodicity is much more dispersed (**Fig. 5a**).
248 This dispersion is consistent with the preference of TFs towards the minor and major grooves
249 of DNA (**Fig. 5b, c**).

250 For example, PITX and EOMES prefer almost opposite phases of nucleosomal DNA
251 (**Fig. 5a**), respectively in phase and out of phase with the TA dinucleotide (**Fig. 5b, c**; the
252 heatmaps). Consistently, the structural analysis indicated their different groove preference:
253 PITX contacts DNA principally by insertions into the major groove (structure in **Fig. 5b**)[48],
254 whereas the T-box TFs principally contact DNA via the minor groove (structure in **Fig. 5c**;
255 see also the references[49,50]). Because the E-MI measure detects the most enriched 3-mer pairs,
256 high E-MI signal usually occurs at positions that correspond to direct TF amino-acid to DNA
257 contacts. Thus, TFs that bind to the major groove tend to show E-MI maximums in phase
258 with TA, and TFs that bind to the minor groove commonly display E-MI maximums out of
259 phase with TA, as seen in **Fig. 5b** and **5c**. Such patterns of TF binding minimize the steric
260 conflict between TF and the histones (cartoon of TF-nucleosome complex in **Fig. 5b, c** and
261 **Extended Data Fig. 6b**).

262 The periodic pattern of E-MI diagonal agrees with the motif matching result
263 (**Extended Data Fig. 6c**). The periodic availability of DNA for TF binding also imposes a
264 ~10 bp periodicity on dimer spacing patterns (**Extended Data Fig. 6d**) for individual TFs
265 that can bind to the outward-facing DNA. However, in most cases such binding appears not
266 to be cooperative, based on the fact that the observed frequency of ligands with two motifs
267 can be well estimated by the frequency of ligands that contain only one motif (data not
268 shown). Taken together, our results indicate TFs tend to bind to the outward-facing side of
269 nucleosomal DNA, as expected from steric considerations.

270 Binding near the nucleosomal dyad

271 Analysis of the positional preference of TFs on nucleosomal DNA also revealed that
272 the region around the nucleosomal dyad is strongly preferred by a few TFs. For example,
273 RFX5 shows the strongest binding around the dyad position of lig147 (**Fig. 6a**, **Extended**
274 **Data Fig. 7a**). Also, multiple SOX TFs show a preference for binding to DNA near the dyad
275 (**Fig. 6b**). Distinct from other regions of nucleosomal DNA, the dyad region contains only a
276 single DNA gyre (**Fig. 6c**), and the histone disk is thinnest there[41,51]. These features of the
277 dyad DNA reduce the steric barrier for TF binding, and could allow TFs that bend DNA upon
278 binding (such as SOX proteins[52]) to deform DNA relatively easily.

279 Binding of SOX11 to sites near the dyad of nucleosome was validated with
280 Electrophoretic Mobility Shift Assay (EMSA). Nucleosomes containing a SOX11 binding
281 sequence identified in the NCAP-SELEX experiment were incubated with increasing

282 amounts of purified SOX11 eDBD. The clear super-shift confirmed the binding of SOX11 to
283 the nucleosome (**Fig. 6d**). The result also indicates that SOX11 does not dissociate the
284 nucleosome upon binding.

285 TFs and their binding positions differ in the ability to dissociate the 286 nucleosome

287 To determine whether TF binding affects the stability of the nucleosome, we
288 performed an additional affinity capture step to separate the nucleosome-bound and
289 dissociated DNA (unbound) after the last NCAP-SELEX cycle (**Fig. 1a;** lig147). As a control
290 experiment, we also allowed the last-cycle nucleosome to dissociate without the presence of
291 TFs. TFs whose binding leads to nucleosome dissociation are expected to have more and
292 stronger binding sites in the unbound library compared to the bound library. Conversely, TFs
293 that stabilize the nucleosome will show the reverse. To evaluate each TF's effect on the
294 stability of the nucleosome, the differential E-MI between its bound and unbound libraries
295 was calculated. Control experiments lacking TFs showed very little effect (**Extended Data**
296 **Fig. 8a**), whereas in the presence of TFs, clear differences in E-MI signals were observed
297 (**Fig. 7a** and **Extended Data Fig. 8a**). We found that most TFs (e.g. CDX1) have stronger E-
298 MI in the unbound library compared to that of the bound library (**Fig. 7a, b**), suggesting that
299 they can facilitate nucleosome dissociation upon binding. However, we also identified a few
300 exceptional TFs whose binding stabilized the nucleosome. These include the T-box TFs, such
301 as TBX2. All three TBX2 replicates had higher E-MI in the bound library (**Fig. 7b**).

302 We also found several cases where different binding modes of the same TF could
303 dissociate nucleosome with a different efficiency (**Extended Data Fig. 8b**). Moreover, many
304 TFs' efficiency to dissociate nucleosome depended on the position of binding. In general, we
305 observed that binding events close to the center of nucleosomal DNA more efficiently
306 dissociated the nucleosome (**Fig. 7a** and **Extended Data Fig. 8a**). Interestingly, some TFs
307 could both stabilize and destabilize nucleosome in a position-dependent way. Most of them
308 tend to facilitate the dissociation of nucleosome when bound close to the center of the
309 nucleosomal DNA, and stabilize the nucleosome when bound to the ends (**Fig. 7a**, brackets).
310 It is possible that TFs bound close to the ends could decrease the DNA flexibility there and
311 subsequently disfavor the dissociation of DNA ends from the histones, which in turn
312 contributes to nucleosome stability. More specifically, some ETS members decrease in their
313 efficiency to dissociate nucleosome or even stabilize nucleosome when they bind very close
314 to the dyad (e.g. the ETV factors and ERG, asterisks in **Fig. 7a**, see also **Fig. 7c**).

315 DISCUSSION

316 It is well established that TFs compete with nucleosomes for available genomic DNA
317 sequences, and that this competition has a major influence on gene expression. Although the
318 DNA binding specificities of many TFs and the nucleosome itself are relatively well
319 characterized[38,42,43,53-60], there is little information on how the nucleosome affects TF binding.
320 In this study, we developed a new method, NCAP-SELEX, for analysis of nucleosome-TF
321 interactions and systematically examined 220 TFs' binding preference on nucleosomal DNA.

322 To identify the binding patterns, we used a mutual-information-based method that can detect
323 enrichment of any sequence pattern along the nucleosomal DNA. This analysis, combined
324 with motif matching, identified five major interaction patterns between TFs and the
325 nucleosome (**Fig. 7d**). The interaction modes include (1) binding spanning both of the two
326 gyres of nucleosomal DNA; (2) orientational preference; (3) end preference; (4) periodic
327 binding; and (5) preferential binding to the dyad region of nucleosomal DNA. Together, these
328 findings reveal a rich landscape of interactions between the two key regulators of genome
329 structure and function—the nucleosome and the sequence-specific DNA binding proteins.

330 **Nucleosomes mask interaction surfaces on DNA**

331 Our results confirmed the previous view[18] that the nucleosome inhibits binding of
332 almost all TFs to DNA. TFs and the nucleosome have long been considered to bind DNA in a
333 mutually exclusive fashion[30,61,62]. However, only in a few individual cases has this prediction
334 been validated using direct biochemical assays[19,63]. Here, we performed an NCAP-SELEX
335 experiment that analyzes TF-nucleosome interactions in the absence of higher order effects,
336 such as chromatin compaction, remodeling or histone modification, which may complicate
337 analysis of the *in vivo* TF-nucleosome interactions. We find that for almost all TFs, less
338 binding occurs in regions that have higher nucleosome occupancy (**Fig. 2a**). This result
339 directly verifies the inhibitory role of the nucleosome. In addition, we observed that although
340 differing in extent, most TFs prefer to bind nucleosomal DNA close to the entry and exit
341 positions (**Fig. 4a**). This positional preference is in line with the probability of spontaneous
342 dissociation (breathing) of nucleosomal DNA, which decreases from the end to the center[64-
343 66]. Therefore, the end-binder class of TFs may only be able to bind to regions of DNA that are
344 dissociated from the nucleosome.

345 Wrapping of DNA around the nucleosome results in masking of one side of the DNA
346 helix, but leaves the other side accessible from solvent. Such masking results in a significant
347 accessibility change along each period (~10.2 bp) of the nucleosomal DNA. Therefore, the
348 nucleosome will directly sterically hinder TFs that bind to long motifs through a continuous
349 interaction with the major or minor groove. In particular, this could block the binding of the
350 C2H2 zinc fingers (**Fig. 4a**, see also the references[26,54,55]). In addition, strong steric hindrance
351 will block binding of proteins that radially cover more than 180° of the DNA circumference.
352 This may explain the observed end preference of, for example, the bZIP family and many
353 bHLH factors (**Fig. 4**, see also the references[26,67]). Moreover, nucleosomal DNA is bent
354 relatively sharply, which could impair TF-DNA contacts if TFs have evolved to specifically
355 bind to free DNA.

356 However, we found that many TFs that bind to short motifs, or to discontinuous
357 motifs, are still able to bind to nucleosomal DNA in a periodic pattern that corresponds to the
358 helical periodicity of DNA. This periodicity was not observed on free DNA, indicating that
359 the occlusion of specific positions by the nucleosome still allows TFs to occupy the
360 remaining sites. Such periodic preference of binding has been reported previously for p53 and
361 the glucocorticoid receptor[68,69], but the prevalence and biochemical basis of this phenomenon
362 was not clear.

363 **Nucleosome leads to asymmetric binding of TFs**

364 Our analysis identified many TFs such as ETS and CREB that have an orientational
365 preference to nucleosome when binding nucleosomal DNA. The asymmetry is also observed
366 for the MNase (**Fig. 3f, Extended Data Fig. 3e**) and DNase I[70] profiles around their *in vivo*
367 binding sites. Such orientational preference is induced by the nucleosome, because the
368 nucleosomal environment breaks the rotational symmetry of DNA. Asymmetric chromatin
369 features have been extensively observed previously by many investigators. These include
370 signatures like nucleosome occupancy[71], chromatin accessibility[70], histone modification[71,72],
371 and the nucleosome signatures[73,74]. As these features are a complex outcome of many active
372 and passive cellular processes, the origin of the observed polarity has been unclear. Our
373 results suggest that at least part of the observed asymmetry in chromatin features next to TF
374 binding sites or across nucleosomes is the direct result of the fact that TFs can interact with
375 the nucleosome in a preferred orientation. In addition, because many TFs, including
376 canonical homeodomains, recognize a near-palindromic site even when they bind DNA
377 asymmetrically, the orientational asymmetry is likely to be more pervasive than what was
378 detected in this study.

379 **Nucleosome as a scaffold**

380 The nucleosome has DNA wrapped around it and acts as a scaffold, facilitating
381 specific binding modes that would display very weak affinity on free DNA. A unique
382 property of the nucleosomal DNA is that at most positions, two DNA gyres are parallel to
383 each other. Moreover, the DNA grooves align across the two nucleosomal DNA gyres[41]. The
384 parallel gyres could specifically associate with TF dimers, or TFs having long recognition
385 helices or multiple DNA binding domains. Here, we found the T-box factors T and TBX2 are
386 using this scaffold to bind nucleosomal DNA. Similar multi-gyre binding has previously been
387 reported for synthetic DNA binder[75] and for large protein complexes involved in chromatin
388 remodeling[76,77]. However, our results are the first demonstration of this mode of binding for
389 sequence-specific DNA binding proteins. The dual-gyre binding is possible only on
390 nucleosomal DNA, and it thus stabilizes the nucleosome from dissociation, and may therefore
391 function to lock a nucleosome in place at a specific position.

392 In addition to the dual-gyre binding mode, we also identified several TFs that prefer
393 to bind at or near the dyad axis. These included RFX5 and five SOX TFs. The dyad region of
394 nucleosomal DNA differs from other nucleosomal DNA in three respects. First, the dyad
395 region contains only a single DNA gyre and thus has a lower steric barrier for binding.
396 Second, the histone disk of the nucleosome is thinnest near the dyad; this further reduces the
397 steric barrier, and also allows TFs to deform the dyad DNA more easily due to a weaker
398 interaction with histones; the higher deformability likely accounts for the dyad preference of
399 SOXs, which bend DNA upon binding. Third, the entry and exit of nucleosomal DNA are
400 also close to the dyad; together with the dyad DNA, they provide a scaffold for specific
401 configurations of TFs. FoxA has been suggested to make use of this scaffold to achieve
402 highly specific positioning close to the dyad[20,78]; this binding mode mimics that of the linker
403 histones H1 and H5[79]. However, the dyad positioning of FoxA is not observed in this study

404 using eDBD, potentially because the full length of FoxA is required for its interaction with
405 the nucleosome[21].

406 Available sites on histones also contribute to part of the nucleosome scaffold. Many
407 proteins bind nucleosomal DNA by contacting both the nucleosomal DNA and the histones,
408 as evidenced for the chromatin remodelers and histone modifiers[51,80,81]. The additional
409 contact with histones will allow proteins to bind nucleosomal DNA with a higher affinity
410 than free DNA, and could also lead to functional histone distortions upon binding[82]. Further
411 structural analyses are necessary to determine whether the positional preferences of, for
412 example, SOXs and RFX5 are resulted from interactions with histone proteins, or are
413 primarily driven by the more accessible nature of the dyad DNA.

414 Pioneer TFs and nucleosome binding

415 Pioneer TFs are defined by their ability to bind nucleosomal DNA[18]. In many cases it
416 is unclear whether such TFs prefer nucleosomal DNA over free DNA, or bind nucleosomal
417 DNA only relatively better than non-pioneer TFs. It is noteworthy that TFs may also facilitate
418 the access of nucleosomal DNA even without displacing the nucleosome, by competing with
419 linker histones and maintaining nucleosome in an accessible conformation[20]. Such a
420 mechanism requires a dyad preference. It is thus of particular interest to further examine the
421 interaction of dyad binders with linker histones.

422 In NCAP-SELEX, we observed that for the eDBD of almost all TFs, including known
423 pioneer factors such as FOX and SOX, binding to free DNA was preferred compared with
424 their binding to nucleosomal DNA. This order of preference results in destabilization of the
425 nucleosomes that are bound by the TFs by mass action. The different binding modes that we
426 identified also differ in their potential for pioneer activity. Whereas end-binders are unable to
427 effectively access nucleosomal DNA, a large fraction of nucleosome-bound DNA sequence
428 will be accessible to the TFs in the periodic binder class. The dyad binders, in turn, can
429 access only highly specific positions along the nucleosomal DNA. Moreover, some TFs have
430 developed "pioneer modes" to bind nucleosomal DNA in a different way compared to their
431 binding to free DNA. For example, the transcription factor T has its normal binding mode
432 inhibited by nucleosome occupancy (**Fig. 3a**, **Extended Data Fig. 2a**). Nonetheless, its dual-
433 gyre binding mode is only allowed on nucleosomal DNA. It is also possible that we did not
434 identify some pioneer TFs, as additional domains in the full-length protein could be required
435 for their high-affinity binding to the nucleosomal DNA. The ability of a large number of TFs
436 to access different positions along the nucleosomal DNA indicates that nucleosomes at
437 different genomic positions are accessible to different classes of TFs, leading to a complex
438 interplay between the DNA sequence, nucleosome positions, and the TF content of a cell.

439 Dissociating the nucleosome

440 The binding of pioneer factors does not necessarily dissociate the nucleosome. But
441 their ability to dissociate nucleosomes is linked to their tendency to open chromatin and to
442 activate transcription. For the libraries enriched by each TF, we examined if the nucleosome
443 is dissociated by comparing the bound and unbound libraries of cycle five. In accord with the

mutually exclusive nature between TF and nucleosome binding, most TFs facilitated the dissociation of nucleosomes. In cells, these TFs are predicted to act passively to dissociate nucleosomes, by having a moderate affinity towards nucleosomal DNA, and high affinity towards free DNA. This mechanism provides favorable kinetics as binding would not require prior dissociation of the nucleosome, and also contributes free energy for displacing the nucleosome. These TFs are thereby potential activators that can open chromatin and regulate gene expression.

Some TFs, in turn, stabilized the nucleosome. These factors could act to repress gene expression, or to precisely position nucleosomes at specific genomic loci. However, in cells, they might also potentially activate an enzymatic process that leads to dissociation, displacement or remodeling of the nucleosome. Moreover, we also observed TFs that both stabilize and destabilize nucleosomal DNA depending on their relative position of binding. Such ability could be used to more precisely position local nucleosomes.

TFs and the nucleosome are central elements regulating eukaryotic gene expression. In this work, we have systematically analyzed the ability of TFs to bind to and to dissociate the nucleosome. The results revealed five distinct modes of TF-nucleosome interactions, including a symmetry-breaking effect induced by the nucleosomal context that is likely to contribute to the extensively observed asymmetric environment around gene regulatory elements. In addition, we discovered major differences in the ability of specific TFs to bind to and open nucleosomal DNA. The identified binding modes explain in part the complexity of the relationship between sequence and gene expression in eukaryotes, and provide a basis for future studies aimed at understanding transcriptional regulation based on biochemical principles.

REFERENCES

1 Andrews, A. J. & Luger, K. Nucleosome structure(s) and stability: variations on a theme. *Annu. Rev. Biophys.* **40**, 99-117 (2011).

2 Segal, E. & Widom, J. What controls nucleosome positions? *Trends Genet.* **25**, 335-343 (2009).

3 Richmond, T. J. & Davey, C. A. The structure of DNA in the nucleosome core. *Nature* **423**, 145-150 (2003).

4 McGinty, R. K. & Tan, S. Nucleosome structure and function. *Chem. Rev.* **115**, 2255-2273 (2015).

5 Valouev, A. *et al.* Determinants of nucleosome organization in primary human cells. *Nature* **474**, 516-520 (2011).

6 Wang, J. P. *et al.* Preferentially quantized linker DNA lengths in Saccharomyces cerevisiae. *PLoS Comput. Biol.* **4**, e1000175 (2008).

7 Felsenfeld, G. & Groudine, M. Controlling the double helix. *Nature* **421**, 448-453 (2003).

8 Jin, J. *et al.* Synergistic action of RNA polymerases in overcoming the nucleosomal barrier. *Nat. Struct. Mol. Biol.* **17**, 745-752 (2010).

9 Natarajan, A., Yardimci, G. G., Sheffield, N. C., Crawford, G. E. & Ohler, U. Predicting cell-type-specific gene expression from regions of open chromatin. *Genome Res.* **22**, 1711-1722 (2012).

10 Raveh-Sadka, T. *et al.* Manipulating nucleosome disfavoring sequences allows fine-tune regulation of gene expression in yeast. *Nat. Genet.* **44**, 743-750 (2012).
11 Teves, S. S., Weber, C. M. & Henikoff, S. Transcribing through the nucleosome. *Trends Biochem. Sci.* **39**, 577-586 (2014).
12 Kireeva, M. L. *et al.* Nucleosome remodeling induced by RNA polymerase II: Loss of the H2A/H2B dimer during transcription. *Mol. Cell* **9**, 541-552 (2002).
13 Hartzog, G. A. Transcription elongation by RNA polymerase II. *Curr. Opin. Genet. Dev.* **13**, 119-126 (2003).
14 Weber, C. M., Ramachandran, S. & Henikoff, S. Nucleosomes are context-specific, H2A.Z-modulated barriers to RNA polymerase. *Mol. Cell* **53**, 819-830 (2014).
15 Gross, D. S. & Garrard, W. T. Nuclease hypersensitive sites in chromatin. *Annu. Rev. Biochem.* **57**, 159-197 (1988).
16 Thurman, R. E. *et al.* The accessible chromatin landscape of the human genome. *Nature* **489**, 75-82 (2012).
17 Neph, S. *et al.* An expansive human regulatory lexicon encoded in transcription factor footprints. *Nature* **489**, 83-90 (2012).
18 Zaret, K. S. & Mango, S. E. Pioneer transcription factors, chromatin dynamics, and cell fate control. *Curr. Opin. Genet. Dev.* **37**, 76-81 (2016).
19 Sekiya, T., Muthurajan, U. M., Luger, K., Tulin, A. V. & Zaret, K. S. Nucleosome-binding affinity as a primary determinant of the nuclear mobility of the pioneer transcription factor FoxA. *Genes Dev.* **23**, 804-809 (2009).
20 Iwafuchi-Doi, M. *et al.* The pioneer transcription factor FoxA maintains an accessible nucleosome configuration at enhancers for tissue-specific gene activation. *Mol. Cell* **62**, 79-91 (2016).
21 Cirillo, L. A. *et al.* Opening of compacted chromatin by early developmental transcription factors HNF3 (FoxA) and GATA-4. *Mol. Cell* **9**, 279-289 (2002).
22 Hsu, H. T. *et al.* Recruitment of RNA polymerase II by the pioneer transcription factor PHA-4. *Science* **348**, 1372-1376 (2015).
23 Iwafuchi-Doi, M. & Zaret, K. S. Cell fate control by pioneer transcription factors. *Development* **143**, 1833-1837 (2016).
24 Iwafuchi-Doi, M. & Zaret, K. S. Pioneer transcription factors in cell reprogramming. *Genes Dev.* **28**, 2679-2692 (2014).
25 Cirillo, L. A. *et al.* Binding of the winged-helix transcription factor HNF3 to a linker histone site on the nucleosome. *EMBO J.* **17**, 244-254 (1998).
26 Soufi, A. *et al.* Pioneer transcription factors target partial DNA motifs on nucleosomes to initiate reprogramming. *Cell* **161**, 555-568 (2015).
27 Segal, E., Raveh-Sadka, T., Schroeder, M., Unnerstall, U. & Gaul, U. Predicting expression patterns from regulatory sequence in Drosophila segmentation. *Nature* **451**, 535-540 (2008).
28 Polach, K. J. & Widom, J. A model for the cooperative binding of eukaryotic regulatory proteins to nucleosomal target sites. *J. Mol. Biol.* **258**, 800-812 (1996).
29 Wasson, T. & Hartemink, A. J. An ensemble model of competitive multi-factor binding of the genome. *Genome Res.* **19**, 2101-2112 (2009).
30 Mirny, L. A. Nucleosome-mediated cooperativity between transcription factors. *Proc. Natl. Acad. Sci. U.S.A.* **107**, 22534-22539 (2010).
31 Kazemian, M., Pham, H., Wolfe, S. A., Brodsky, M. H. & Sinha, S. Widespread evidence of cooperative DNA binding by transcription factors in Drosophila development. *Nucleic Acids Res.* **41**, 8237-8252 (2013).
32 Vashee, S., Melcher, K., Ding, W. V., Johnston, S. A. & Kodadek, T. Evidence for two modes of cooperative DNA binding in vivo that do not involve direct protein-protein interactions. *Curr. Biol.* **8**, 452-458 (1998).
33 Moyle-Heyrman, G., Tims, H. S. & Widom, J. Structural constraints in collaborative competition of transcription factors against the nucleosome. *J. Mol. Biol.* **412**, 634-646 (2011).

542 34 Boyer, L. A. *et al.* Core transcriptional regulatory circuitry in human embryonic stem
543 cells. *Cell* **122**, 947-956 (2005).
544 35 Roy, S. *et al.* Identification of functional elements and regulatory circuits by
545 Drosophila modENCODE. *Science* **330**, 1787-1797 (2010).
546 36 Stanojevic, D., Small, S. & Levine, M. Regulation of a segmentation stripe by
547 overlapping activators and repressors in the Drosophila embryo. *Science* **254**, 1385-
548 1387 (1991).
549 37 Yan, J. *et al.* Transcription factor binding in human cells occurs in dense clusters
550 formed around cohesin anchor sites. *Cell* **154**, 801-813 (2013).
551 38 Jolma, A. *et al.* DNA-dependent formation of transcription factor pairs alters their
552 binding specificity. *Nature* **527**, 384-388 (2015).
553 39 Dyer, P. N. *et al.* Reconstitution of nucleosome core particles from recombinant
554 histones and DNA. *Methods Enzymol.* **375**, 23-44 (2004).
555 40 Satchwell, S. C., Drew, H. R. & Travers, A. A. Sequence periodicities in chicken
556 nucleosome core DNA. *J. Mol. Biol.* **191**, 659-675 (1986).
557 41 Luger, K., Mader, A. W., Richmond, R. K., Sargent, D. F. & Richmond, T. J. Crystal
558 structure of the nucleosome core particle at 2.8 A resolution. *Nature* **389**, 251-260
559 (1997).
560 42 Struhl, K. & Segal, E. Determinants of nucleosome positioning. *Nat. Struct. Mol. Biol.*
561 **20**, 267-273 (2013).
562 43 Brogaard, K., Xi, L. Q., Wang, J. P. & Widom, J. A map of nucleosome positions in
563 yeast at base-pair resolution. *Nature* **486**, 496-501 (2012).
564 44 Vaquerizas, J. M., Kummerfeld, S. K., Teichmann, S. A. & Luscombe, N. M. A
565 census of human transcription factors: function, expression and evolution. *Nat. Rev.*
566 *Genet.* **10**, 252-263 (2009).
567 45 Henikoff, J. G., Belsky, J. A., Krassovsky, K., MacAlpine, D. M. & Henikoff, S.
568 Epigenome characterization at single base-pair resolution. *Proc. Natl. Acad. Sci.*
569 *U.S.A.* **108**, 18318-18323 (2011).
570 46 Isaac, R. S. *et al.* Nucleosome breathing and remodeling constrain CRISPR-Cas9
571 function. *Elife* **5**, e13450 (2016).
572 47 Poirier, M. G., Bussiek, M., Langowski, J. & Widom, J. Spontaneous access to DNA
573 target sites in folded chromatin fibers. *J. Mol. Biol.* **379**, 772-786 (2008).
574 48 Chaney, B. A., Clark-Baldwin, K., Dave, V., Ma, J. & Rance, M. Solution structure of
575 the k50 class homeodomain PITX2 bound to DNA and implications for mutations that
576 cause Rieger syndrome. *Biochemistry* **44**, 7497-7511 (2005).
577 49 Stirnimann, C. U., Ptchelkine, D., Grimm, C. & Muller, C. W. Structural basis of
578 TBX5-DNA recognition: the T-Box domain in its DNA-bound and -unbound form. *J.*
579 *Mol. Biol.* **400**, 71-81 (2010).
580 50 Coll, M., Seidman, J. G. & Muller, C. W. Structure of the DNA-bound T-box domain of
581 human TBX3, a transcription factor responsible for ulnar-mammary syndrome.
582 *Structure* **10**, 343-356 (2002).
583 51 McGinty, R. K. & Tan, S. Recognition of the nucleosome by chromatin factors and
584 enzymes. *Curr. Opin. Struct. Biol.* **37**, 54-61 (2016).
585 52 Privalov, P. L., Dragan, A. I. & Crane-Robinson, C. The cost of DNA bending. *Trends*
586 *Biochem. Sci.* **34**, 464-470 (2009).
587 53 Badis, G. *et al.* Diversity and complexity in DNA recognition by transcription factors.
588 *Science* **324**, 1720-1723 (2009).
589 54 Yin, Y. *et al.* Impact of cytosine methylation on DNA binding specificities of human
590 transcription factors. *Science* **356**, eaaj2239 (2017).
591 55 Jolma, A. *et al.* DNA-binding specificities of human transcription factors. *Cell* **152**,
592 327-339 (2013).
593 56 Hughes, A. L. & Rando, O. J. Mechanisms underlying nucleosome positioning in
594 vivo. *Annu. Rev. Biophys.* **43**, 41-63 (2014).
595 57 Radman-Livaja, M. & Rando, O. J. Nucleosome positioning: how is it established,
596 and why does it matter? *Dev. Biol.* **339**, 258-266 (2010).

597 58 Fernandez, A. G. & Anderson, J. N. Nucleosome positioning determinants. *J. Mol.*
598 *Biol.* **371**, 649-668 (2007).
599 59 Kaplan, N. *et al.* The DNA-encoded nucleosome organization of a eukaryotic
600 genome. *Nature* **458**, 362-366 (2009).
601 60 Olson, W. K. & Zhurkin, V. B. Working the kinks out of nucleosomal DNA. *Curr. Opin.*
602 *Struct. Biol.* **21**, 348-357 (2011).
603 61 Ramachandran, S. & Henikoff, S. Transcriptional regulators compete with
604 nucleosomes post-replication. *Cell* **165**, 580-592 (2016).
605 62 Li, M. *et al.* Dynamic regulation of transcription factors by nucleosome remodeling.
606 *Elife* **4**, e06249 (2015).
607 63 Hayes, J. J. & Wolffe, A. P. Histones H2A/H2B inhibit the interaction of transcription
608 factor IIIA with the Xenopus borealis somatic 5S RNA gene in a nucleosome. *Proc.*
609 *Natl. Acad. Sci. U.S.A.* **89**, 1229-1233 (1992).
610 64 Polach, K. J. & Widom, J. Mechanism of protein access to specific DNA sequences
611 in chromatin: a dynamic equilibrium model for gene regulation. *J. Mol. Biol.* **254**, 130-
612 149 (1995).
613 65 Anderson, J. D. & Widom, J. Sequence and position-dependence of the equilibrium
614 accessibility of nucleosomal DNA target sites. *J. Mol. Biol.* **296**, 979-987 (2000).
615 66 Li, G., Levitus, M., Bustamante, C. & Widom, J. Rapid spontaneous accessibility of
616 nucleosomal DNA. *Nat. Struct. Mol. Biol.* **12**, 46-53 (2005).
617 67 Jones, S. An overview of the basic helix-loop-helix proteins. *Genome Biol.* **5**, 226
618 (2004).
619 68 Cui, F. & Zhurkin, V. B. Rotational positioning of nucleosomes facilitates selective
620 binding of p53 to response elements associated with cell cycle arrest. *Nucleic Acids*
621 *Res.* **42**, 836-847 (2014).
622 69 Li, Q. & Wrange, O. Accessibility of a glucocorticoid response element in a
623 nucleosome depends on its rotational positioning. *Mol. Cell. Biol.* **15**, 4375-4384
624 (1995).
625 70 Sherwood, R. I. *et al.* Discovery of directional and nondirectional pioneer transcription
626 factors by modeling DNase profile magnitude and shape. *Nat. Biotechnol.* **32**, 171-
627 178 (2014).
628 71 Kundaje, A. *et al.* Ubiquitous heterogeneity and asymmetry of the chromatin
629 environment at regulatory elements. *Genome Res.* **22**, 1735-1747 (2012).
630 72 Dunham, I. *et al.* An integrated encyclopedia of DNA elements in the human genome.
631 *Nature* **489**, 57-74 (2012).
632 73 Gonzalez, S. *et al.* Nucleosomal signatures impose nucleosome positioning in coding
633 and noncoding sequences in the genome. *Genome Res.* **26**, 1532-1543 (2016).
634 74 Quintales, L., Soriano, I., Vazquez, E., Segurado, M. & Antequera, F. A species-
635 specific nucleosomal signature defines a periodic distribution of amino acids in
636 proteins. *Open Biology* **5**, 140218 (2015).
637 75 Edayathumangalam, R. S., Weyermann, P., Gottesfeld, J. M., Dervan, P. B. & Luger,
638 K. Molecular recognition of the nucleosomal "supergroove". *Proc. Natl. Acad. Sci.*
639 *U.S.A.* **101**, 6864-6869 (2004).
640 76 Richmond, T. J. Nucleosome recognition and spacing by chromatin remodelling
641 factor ISW1a. *Biochem. Soc. Trans.* **40**, 347-350 (2012).
642 77 Nodelman, I. M. *et al.* Interdomain communication of the Chd1 chromatin remodeler
643 across the DNA gyres of the nucleosome. *Mol. Cell* **65**, 447-459 (2017).
644 78 Ye, Z. Q. *et al.* Genome-wide analysis reveals positional-nucleosome-oriented
645 binding pattern of pioneer factor FOXA1. *Nucleic Acids Res.* **44**, 7540-7554 (2016).
646 79 Bednar, J. *et al.* Structure and dynamics of a 197 bp nucleosome in complex with
647 linker histone H1. *Mol. Cell* **66**, 384-397 (2017).
648 80 Makde, R. D., England, J. R., Yennawar, H. P. & Tan, S. Structure of RCC1
649 chromatin factor bound to the nucleosome core particle. *Nature* **467**, 562-566 (2010).

81 Armache, K. J., Garlick, J. D., Canzio, D., Narlikar, G. J. & Kingston, R. E. Structural basis of silencing: Sir3 BAH domain in complex with a nucleosome at 3.0 Å resolution. *Science* **334**, 977-982 (2011).
82 Sinha, K. K., Gross, J. D. & Narlikar, G. J. Distortion of histone octamer core promotes nucleosome mobilization by a chromatin remodeler. *Science* **355**, eaaa3761 (2017).
83 Sagendorf, J. M., Berman, H. M. & Rohs, R. DNAproDB: an interactive tool for structural analysis of DNA-protein complexes. *Nucleic Acids Res.*, doi: 10.1093/nar/gkx1272 (2017).
84 Zhang, J. J., Kobert, K., Flouri, T. & Stamatakis, A. PEAR: a fast and accurate Illumina Paired-End reAd mergeR. *Bioinformatics* **30**, 614-620 (2014).
85 Gu, Z., Gu, L., Eils, R., Schlesner, M. & Brors, B. *circlize* Implements and enhances circular visualization in R. *Bioinformatics* **30**, 2811-2812 (2014).
86 Korhonen, J., Martinmaki, P., Pizzi, C., Rastas, P. & Ukkonen, E. MOODS: fast search for position weight matrix matches in DNA sequences. *Bioinformatics* **25**, 3181-3182 (2009).
87 Pizzi, C., Rastas, P. & Ukkonen, E. Finding significant matches of position weight matrices in linear time. *IEEE/ACM Trans. Comput. Biol. Bioinform.* **8**, 69-79 (2011).
88 Nitta, K. R. *et al.* Conservation of transcription factor binding specificities across 600 million years of bilateria evolution. *Elife* **4**, e04837 (2015).
89 Slattery, M. *et al.* Cofactor binding evokes latent differences in DNA binding specificity between Hox proteins. *Cell* **147**, 1270-1282 (2011).
90 Riley, T. R. *et al.* SELEX-seq: a method for characterizing the complete repertoire of binding site preferences for transcription factor complexes. *Methods Mol. Biol.* **1196**, 255-278 (2014).
91 Mieczkowski, J. *et al.* MNase titration reveals differences between nucleosome occupancy and chromatin accessibility. *Nat. Commun.* **7**, 11485 (2016).
92 Li, H. & Durbin, R. Fast and accurate short read alignment with Burrows-Wheeler transform. *Bioinformatics* **25**, 1754-1760 (2009).
93 Lowary, P. T. & Widom, J. New DNA sequence rules for high affinity binding to histone octamer and sequence-directed nucleosome positioning. *J. Mol. Biol.* **276**, 19-42 (1998).
94 Collings, C. K., Fernandez, A. G., Pitschka, C. G., Hawkins, T. B. & Anderson, J. N. Oligonucleotide sequence motifs as nucleosome positioning signals. *PLoS ONE* **5**, e10933 (2010).
95 Jolma, A. *et al.* Multiplexed massively parallel SELEX for characterization of human transcription factor binding specificities. *Genome Res.* **20**, 861-873 (2010).

691 ## END NOTES

692 **Supplementary Information** is linked to the online version of the paper at
693 www.nature.com/nature.

694

695 **Acknowledgments** We thank Biswajyoti Sahu, Fan Zhong, Kazuhiro Nitta, Arttu Jolma,
696 Minna Taipale, Bei Wei, Jilin Zhang, Ekaterina Morgunova, and Jarkko Toivonen for their
697 valuable suggestions. We thank Lijuan Hu, Jianping Liu, and Sandra Augsten for technical
698 assistance. We thank the ENCODE Consortium and the ENCODE production laboratories for
699 generating the ChIP-seq datasets. This work was supported by Center for Innovative
700 Medicine at Karolinska Institutet, Knut and Alice Wallenberg Foundation, Göran Gustafsson
701 Foundation and Vetenskapsrådet. P.C. was supported by the Deutsche
702 Forschungsgemeinschaft (SFB860, SPP1935), the European Research Council Advanced
703 Investigator Grant TRANSREGULON (grant agreement No 693023), and the Volkswagen
704 Foundation.

705

706 **Author Contributions** J.T., F.Z. and P.C. conceived the experiments. F.Z. performed the
707 NCAP-SELEX, MNase-seq and data analysis. L.F produced the histone octamers. Y.Y.
708 helped with the curation and production of TF proteins. E.K. analysed the MNase-seq data.
709 S.D. performed EMSA validation for SOX. F.J. and J.T. interpreted the data and wrote the
710 manuscript. All authors discussed the findings and contributed to the manuscript.

711

712 **Author Information** All next generation sequencing data will be deposited to European
713 Nucleotide Archive (ENA) under Accession PRJEB22684. All computer programs and
714 scripts used are either published or available upon request. The authors declare no competing
715 financial interests. Requests for materials should be addressed to J.T. (jussi.taipale@ki.se).

716

717 **FIGURE LEGENDS**

Figure 1, Zhu et al. 2017

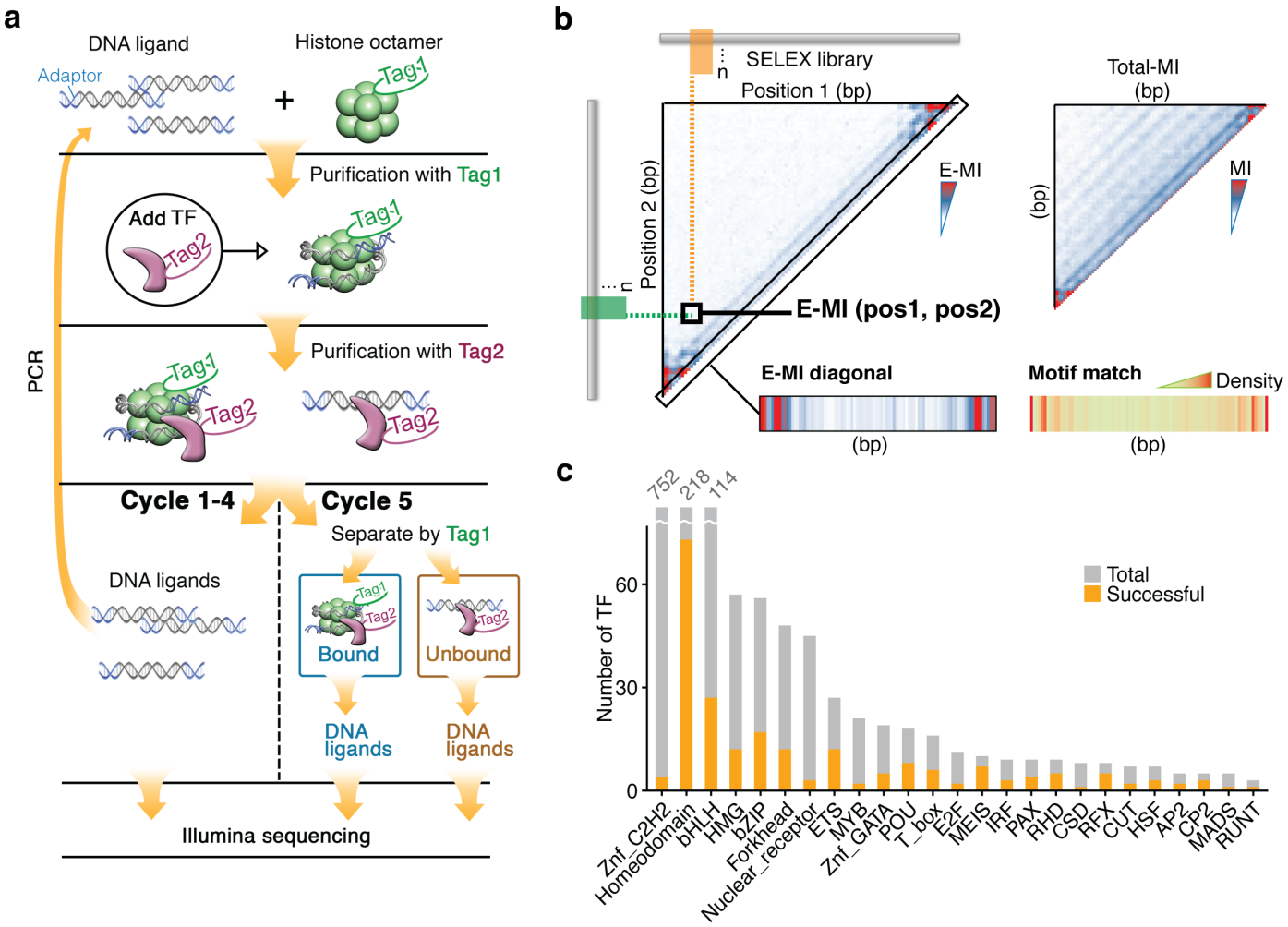

718

719 **Figure 1 | Nucleosome CAP-SELEX**. **a,** Schematic representation of NCAP-SELEX. The
720 DNA ligands for SELEX contain a randomized region (grey) with fixed adaptors (blue) at
721 both ends. The protocol first selects for ligands that are favored by the nucleosome, and then
722 from the nucleosome-bound ligand pool selects for ligands that bind to a given TF. The
723 orthogonal tagging of histone H2A (tag1) and TFs (tag2) enables the consecutive affinity
724 purification. In the last (5th) cycle, the TF-bound DNA ligands are further separated into
725 nucleosome-bound and unbound libraries. **b,** TF-signal analysis by E-MI. For the library
726 enriched by each TF, E-MI (Mutual Information between the most Enriched 3-mer pairs) is
727 calculated pairwise between all non-overlapping 3-mer columns (left triangle). When
728 analysing TF signals, we chose E-MI instead of total-MI (right triangle) because total-MI
729 detects also signals from the nucleosome (the stripes with 10-bp intervals). The diagonal of
730 the E-MI plot (bottom left) is most informative, and is generally in line with the motif-
731 matching result (bottom right). **c,** Family-wise coverage of successful TFs.

Figure 2, Zhu et al. 2017

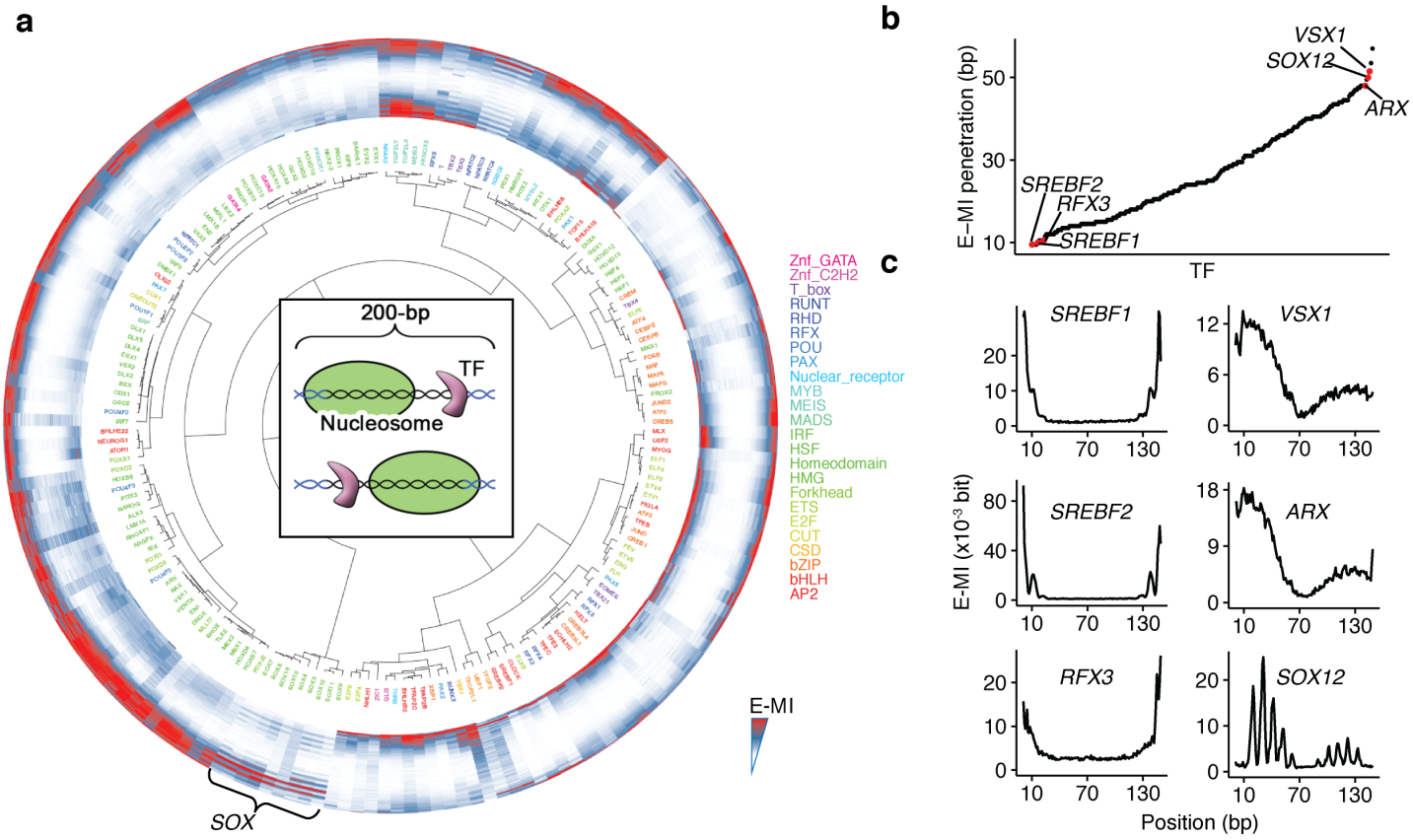

732

733 **Figure 2 | Nucleosomal DNA is less accessible for TFs than free DNA**. **a,** Hierarchical
734 clustering of the E-MI diagonals for NCAP-SELEX with the 200-bp ligand (lig200). The E-
735 MI diagonal for each TF is oriented radially. The names of the TFs are colored by family
736 with the coloring scheme indicated on the right. TFs from the same family tend to be
737 clustered together (e.g., SOX, indicated). The illustration at the center of the dendrogram
738 schematically represents TF's binding on lig200. Note that almost all TFs have lower E-MI
739 towards the center of lig200, indicating their lower affinity to nucleosomal DNA compared
740 with free DNA. The E-MI diagonals are scaled for each TF. **b,** E-MI penetration of individual
741 TFs on lig200. TFs are ordered according to their E-MI penetration depth towards the center
742 of the ligand. This order reflects TFs' ability to bind nucleosome-occupied DNA. Six TFs
743 representing either of the two extremes are colored red and exemplified in (**c**). **c,** The
744 diagonal of E-MI for TFs with highest/lowest E-MI penetrations. Left: TFs with lowest E-MI
745 penetrations; right: TFs with highest E-MI penetrations.

746

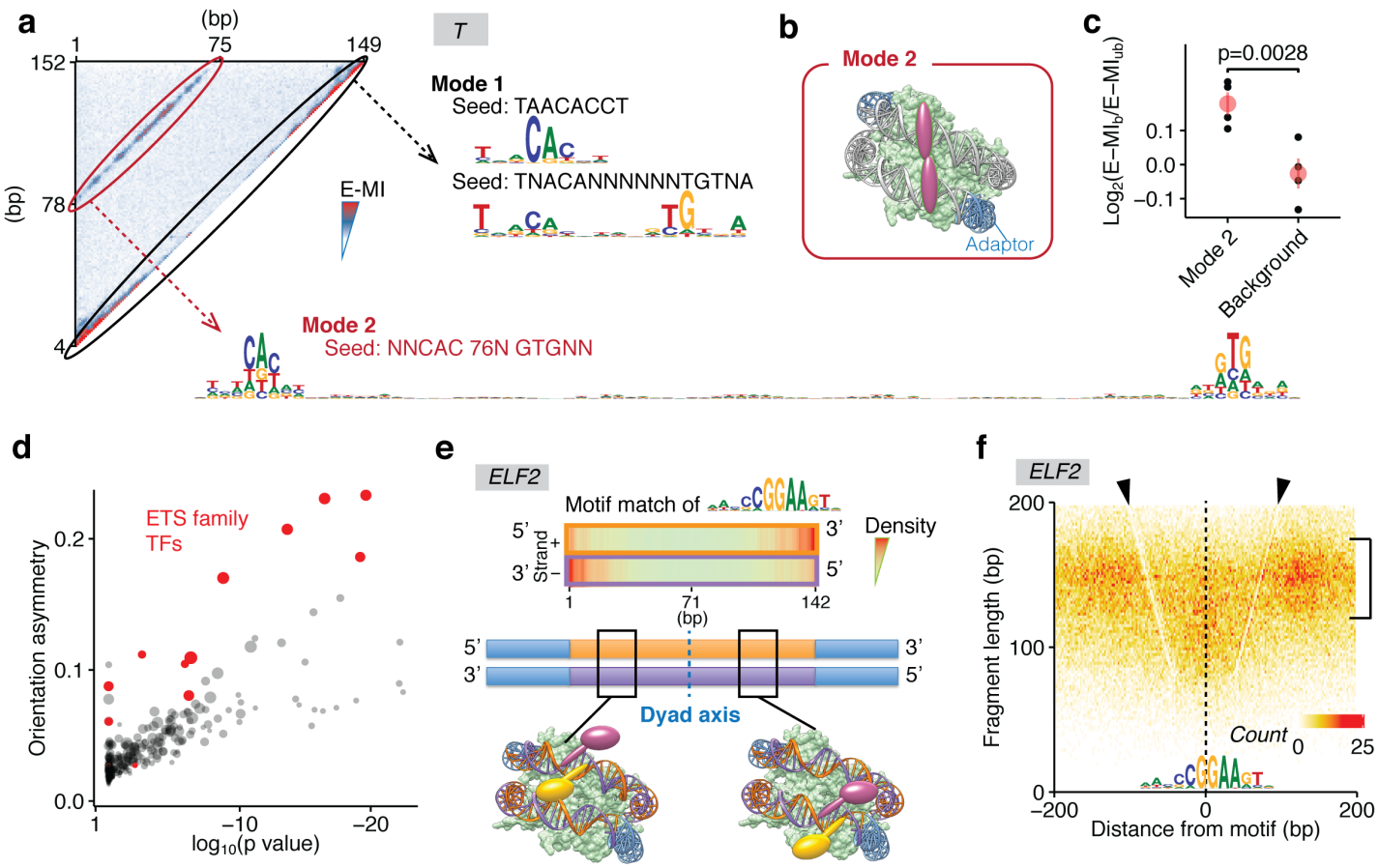

Figure 3 | Nucleosome allows binding that spans two gyres and breaks the rotational symmetry of DNA. a, Two modes used by T (brachyury) to bind nucleosomal DNA. The heatmap shows the pairwise E-MI for all combinations of positions on the 200-bp ligand. The Mode 1 signal near the diagonal gives motifs similar to those seen on the free DNA. The Mode 2 signal corresponds to a ~80-bp-long motif. Mode 1 is inhibited by higher nucleosome occupancy towards the center whereas Mode 2 gets stronger in the middle. Seed for each motif is also indicated. **b,** Schematic representation of TFs that bind the two gyres of nucleosomal DNA at the same time. **c,** Mode 2 binding stabilizes nucleosome from dissociation. Log2 ratio of E-MI between the bound and unbound libraries (cycle five, four replicates) of T is calculated for both the Mode 2 binding and the background E-MI level (see **Method** for details). The bound library has stronger Mode 2 binding but similar background. Each point indicates a replicate. Data are mean ± s.d.; two-sided t-test was used, 95% CI, 0.097–0.202. **d,** Orientational asymmetry of individual TFs. For each TF, the asymmetry is evaluated by the binding energy difference between the two relative orientations, averaged for 40 non-palindromic 8-mers that are most enriched in the TF's NCAP-SELEX library; significance of the asymmetry is also tested to obtain the p value (see **Method** for details). Most of the ETS-family TFs (red) show a prominent orientational asymmetry. Dot size represents the extent of signal enrichment in each TF's NCAP-SELEX library. **e,** The orientational asymmetry of ELF2. The ETS factor ELF2 has different motif density

767 distributions for the two strands of nucleosomal DNA (top panel). This is because at a
768 specific position, TFs (magenta and yellow, bottom panel) that respectively bind to motifs on
769 different DNA strands (purple and orange, blue for constant adaptor region) will differ in
770 their surrounding chemical environments. For motifs that locate on different DNA strands
771 and equidistant from the dyad, their chemical environment for binding will be identical due to
772 the rotational symmetry of the nucleosome (with respect to the dyad axis), e.g., the magenta
773 TF in the left model has the same chemical environment as the yellow TF in the right model.
774 As a result, the motif densities on two DNA strands are different but symmetric to each other
775 with regard to the dyad. **f,** The asymmetric MNase fragment profile around genomic ELF2
776 sites. ELF2 motif matches within ChIP-seq peaks were positioned at the center. Nearby
777 MNase fragment counts are summarized with 2 × 2 bins according to their lengths and center
778 positions. Nucleosome distribution near the ELF2 sites are reflected by the signal intensity of
779 the ~150 bp fragments (bracket). The V-shaped lines with a lower signal intensity
780 (arrowheads) reveal the footprint of the TF, which is asymmetric.

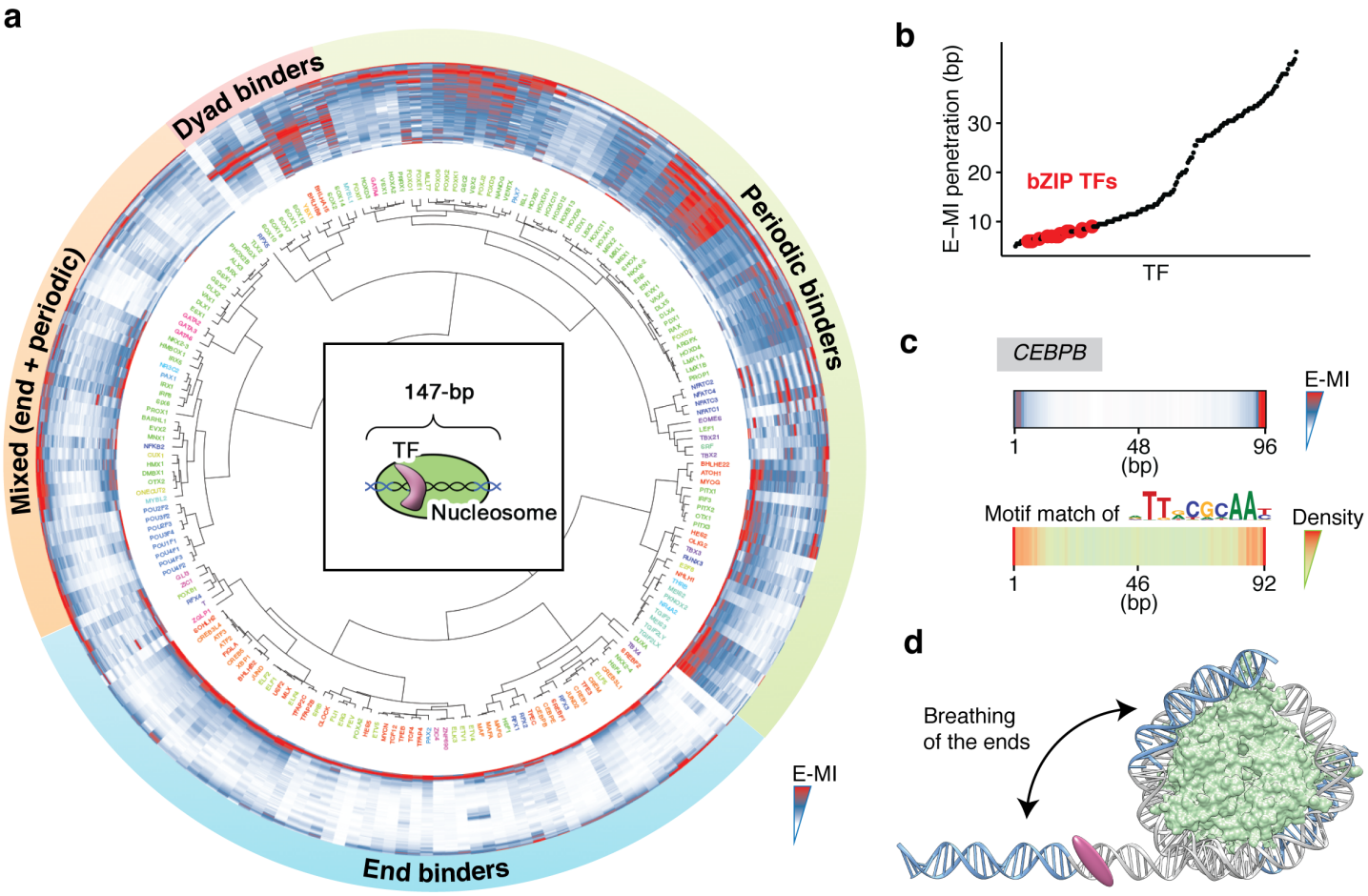

781

782 **Figure 4 | Nucleosome induces positional preference to TF binding. a,** Hierarchical
783 clustering of the E-MI diagonals for NCAP-SELEX with the 147-bp ligand (lig147). The
784 coloring scheme is the same as that in **Fig. 2a**. In the center of the dendrogram, the schematic
785 shows that nucleosome is positioned uniquely on lig147. TFs are assigned to three separate
786 classes and a mixed class. E-MI diagonal is scaled for each TF. **b,** E-MI penetration of each
787 TF on lig147. All examined bZIP TFs are marked with red. Their low penetrations indicate
788 an end preference. **c,** E-MI diagonal and motif matching results for the bZIP factor CEBPB.
789 **d,** Schematic representation showing a TF is preferring the ends of nucleosomal DNA due to
790 breathing. Both the two ends of nucleosomal DNA will breath but only one is illustrated here
791 for clarity.

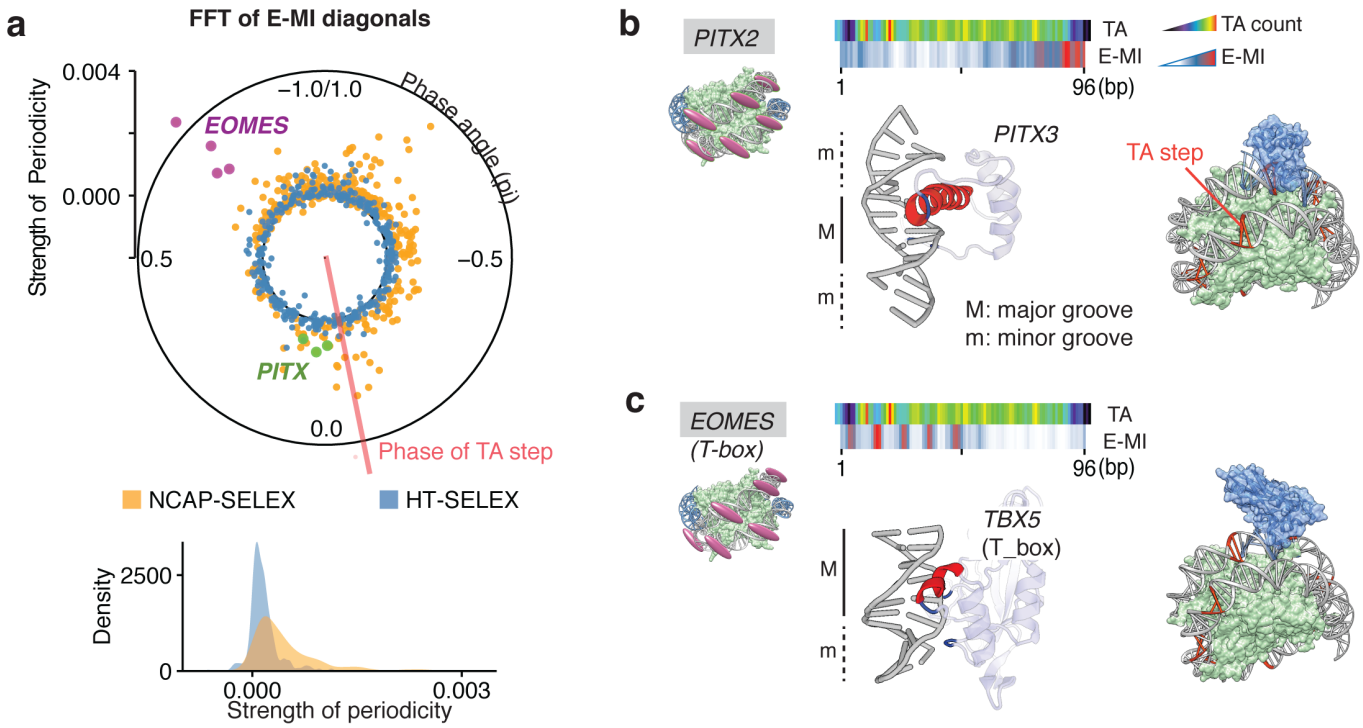

Figure 5 | Periodic binding of TFs to the major or minor grooves facing outwards. **a,** Strength and phase of the ~10 bp periodicity for individual TFs. The polar plot shows the strength and phase of the periodicity derived from the FFT of E-MI diagonals; data for both the NCAP-SELEX (orange; nucleosomal DNA) and the HT-SELEX (blue; free DNA) are shown. Each dot represents one SELEX library. EOMES (magenta, four replicates) and PITX (green for PITX1, 2, 3) have opposite phases; they are exemplified in (**b**, **c**). The phase of the TA dinucleotide (red line, median value of all NCAP-SELEX libraries) is also shown to indicate where histones contact nucleosomal DNA[42]. Bottom: density plot of the periodicity strength for all TFs. **b,** Major groove binder prefers exposed major grooves on nucleosomal DNA. The E-MI diagonal of PITX is in phase with the TA peaks along the ligand. The structure of PITX (PDB 2lkx, visualized with DNAproDB[83]) also show contacts with DNA principally in the major groove (M). The base-contacting helices (red) and loops (blue) are indicated. Cartoon representation to the right shows that the steric hindrance is minimal when PITX (blue) binds in phase with TA (orange) on the nucleosome structure (PDB 3ut9). **c,** Minor groove binder prefers exposed minor grooves (m) on nucleosomal DNA. The E-MI diagonal of EOMES (T-box) is out of phase with the TA peaks, suggesting it binds positions where nucleosomal DNA's minor groove is facing outside. The TBX5 (T-box) structure (PDB 2x6v) also shows contacts with DNA principally in the minor groove. Cartoon representation to the right shows that the steric hindrance is minimal when TBX5 (blue) binds out of phase with TA (orange) on the nucleosome structure (PDB 3ut9).

Figure 6, Zhu et al. 2017

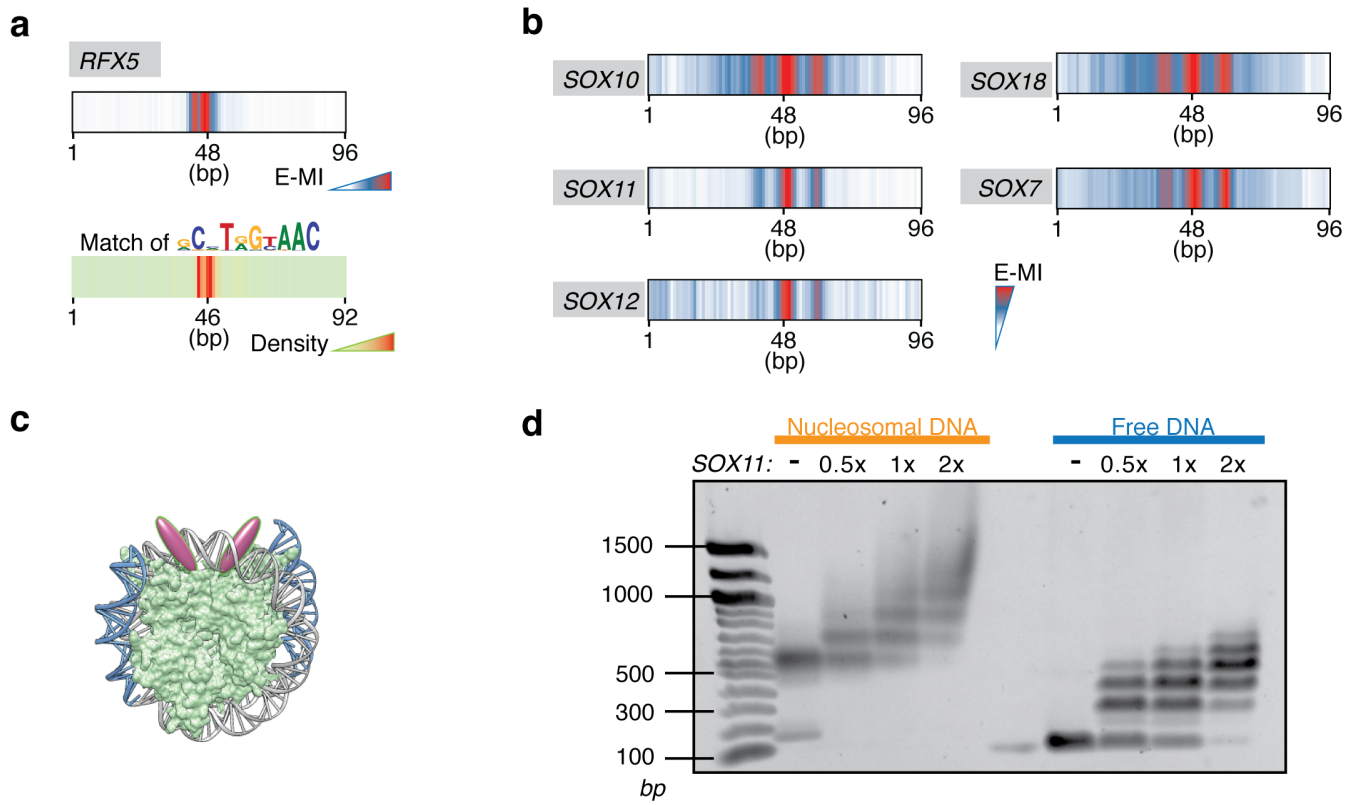

Figure 6 | Binding near the dyad axis. **a,** E-MI diagonal and motif matching results for RFX5. **b,** E-MI diagonal of SOX family TFs showing their preferred binding around the dyad. **c,** Schematic representation of TFs that prefer to bind around the dyad. **d,** EMSA of SOX11 complexes with nucleosome and with free DNA. Nucleosome is reconstituted and purified using a modified Widom 601 sequence, which contains a SOX11 binding sequence (extracted from cycle 4 SELEX library) embedded close to the dyad. Each 40 µl reaction contains 1 µg DNA, together with SOX11 protein at a molar ratio of 0, 0.5, 1, 2 (indicated on top of each lane) to DNA.

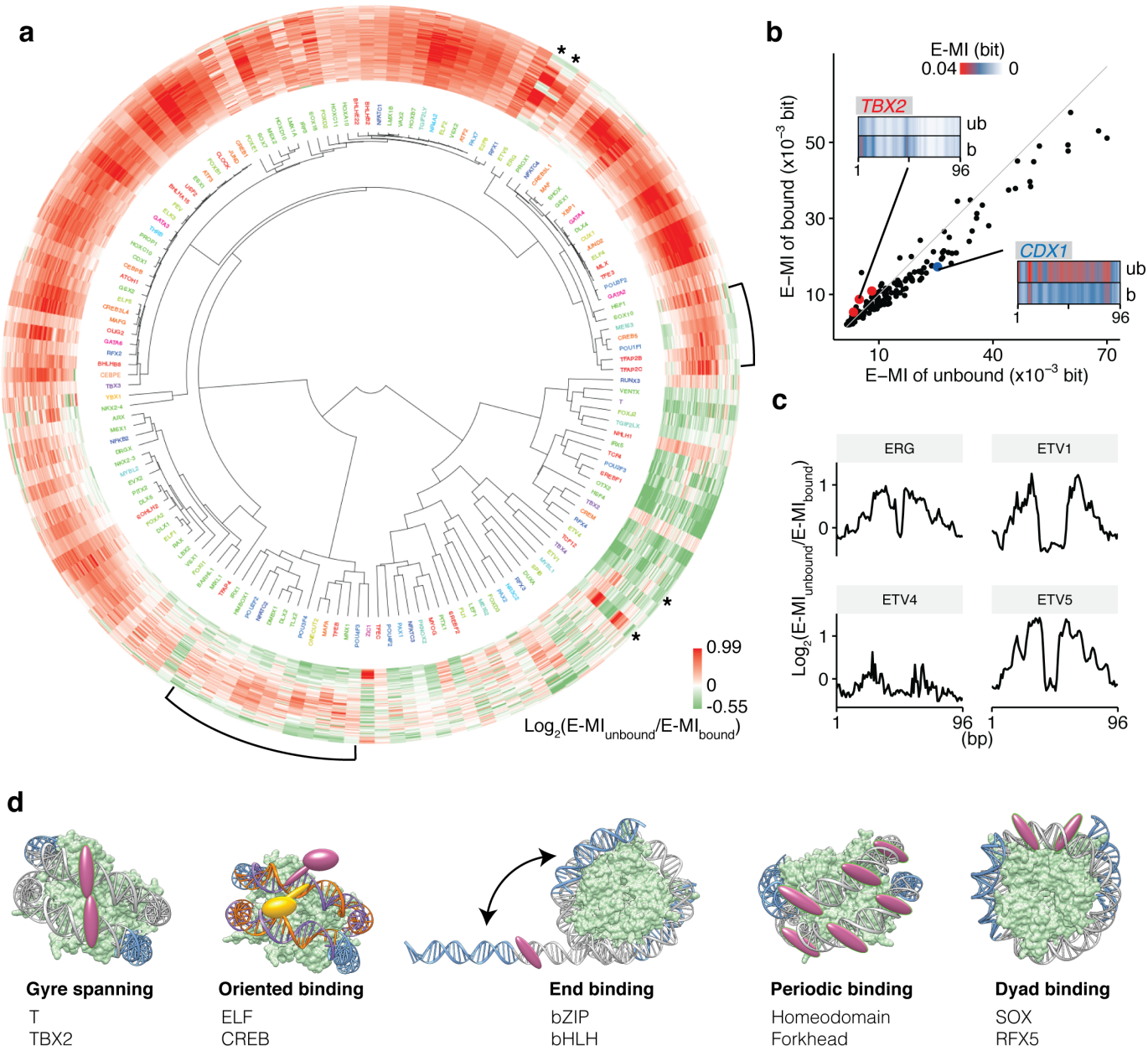

Figure 7 | Effects of TF binding on nucleosome stability and a summary of identified TF-nucleosome interaction modes. a, Hierarchical clustering of the differential E-MI diagonal between the bound and the unbound cycle 5 libraries. TF names are colored to encode their family information (coloring scheme as indicated in **Fig. 2a**). Brackets denote TFs that both destabilize and stabilize nucleosome in a position-dependent way. Asterisks denote the ETS factors with a specific pattern of positional dependence. **b,** Mean strengths of E-MI diagonals in the bound and the unbound cycle 5 libraries. The scatterplot shows the mean E-MI for the diagonals of each TF (dots), and for both the bound library (*y* axis) and the unbound library (*x* axis). The grey line represents where *y*=*x*. Most TFs have stronger signals in the unbound library (e.g. CDX1, blue). A few TFs show the reverse (e.g. TBX2, red). For CDX1 and TBX2 the E-MI diagonals of the bound (b) and the unbound (ub) libraries are also illustrated. **c,** Differential E-MI diagonals for the four ETS family TFs indicated by asterisks in (**a**). **d,** The identified major interaction modes of TFs with nucleosomal DNA.

838 # METHODS

839 ## Preparation of histone octamer

840 A vector encoding *Xenopus laevis* H2A with an N-terminal tag was cloned using
841 'Round-the-horn site-directed mutagenesis. *X. laevis* histones were expressed and purified as
842 described previously[39]. Inclusion bodies were resuspended by using a Dounce tissue grinder
843 (Sigma-Aldrich). Purified histones were aliquoted, flash-frozen, lyophilized, and stored at -
844 80 °C prior to use. The lyophilized histones were resuspended in unfolding buffer (7 M
845 guanidine hydrochloride and 10 mM DTT in 20 mM Tris-Cl, pH 7.5) to a concentration of
846 1.5 mg/ml. N-terminally tagged H2A, H2B, H3 and H4 were then combined at a molar ratio
847 of 1.2:1.2:1:1. The sample was incubated on ice for 30 minutes before it was dialyzed against
848 three times 600 ml refolding buffer (2 M NaCl, 1 mM EDTA, and 5 mM β-mercaptoethanol
849 in 10 mM Tris-Cl, pH 7.5). The sample was recovered after dialysis and applied to a GE
850 S200 16/600 pg size exclusion column (GE Healthcare, Little Chalfont, United Kingdom).
851 Peak fractions were analyzed by SDS-PAGE. Fractions containing the octamer were pooled
852 and concentrated. Both the histone expression and octamer formation have been quality-
853 controlled (**Extended Data Fig. 1a, b**).

854 ## Clones, protein expression and purification for TFs

855 Gateway recipient vectors having a pETG20A backbone were employed in the
856 bacterial protein expression. Insertions for these expression vectors were derived either from
857 PCR clones or from gene synthesis; the details are given by Yin *et al.*[54]. The sequences and
858 domains for all TFs are listed in **Supplementary Table 1**. The non-full-length constructs
859 contain extended DNA binding domains (eDBDs), with a design rationale reported
860 previously[38]. We essentially followed Yin *et al.*[54] to express and purify the proteins from *E.*
861 *coli* cells.

862 ## Nucleosome CAP-SELEX

863 The Nucleosome CAP-SELEX (NCAP-SELEX) protocol has two steps of selection,
864 respectively for ligands bound by the nucleosome and by individual TFs. The DNA ligands
865 were designed based on Illumina's Truseq library (**Supplementary Table 2**). The adapter
866 lengths were 24 bp at the left side and 22 bp at the right side. The total lengths of the ligands
867 are 147 bp for lig147, and 200 bp for lig200, with 101 bp and 154 bp in random, respectively.
868 The single-stranded oligos of lig147 and lig200 were purchased from IDT (Ultramer DNA
869 oligos). A PCR reaction with primers binding to the adapters (**Supplementary Table 2**,
870 PCR_primers) was used to obtain double-stranded DNA from the synthetic oligos, and was
871 also used to amplify the libraries between SELEX cycles. For sequencing, the ligands were
872 amplified with the multiplexing primers (**Supplementary Table 2**, PE_PCR_primers).

873 In SELEX, first, double-stranded DNA ligand and tagged histone octamer were mixed
874 in 2 M KCl solution and incubated for 30 min. The mixture was then diluted stepwise as
875 described by Dyer *et al.*[39], with a dilution buffer (TE buffer supplemented with 1 mM tris(2-
876 carboxyethyl)phosphine (TCEP) and a cocktail of protease inhibitors (05892970001,
877 Roche)). The reconstituted nucleosome was incubated for 30 min with the corresponding

878 affinity beads (pre-blocked with the blocking buffer containing 25mM Tris, 0.5% BSA, 0.1%
879 tween 20, 0.02% NaN_3), and at the same time shaken under 1900 rpm with a microplate
880 shaker (13500-890, VWR). The beads were then washed 15 times with a microplate washer
881 (Hydrospeed^{TM}, Tecan). The nucleosome was eluted and incubated with 10–200 ng purified
882 TFs for 20 min. The TF-bound species were pulled down with magnetic beads (pre-blocked
883 with the blocking buffer) and washed 15 times. The bead suspension were used for PCR as
884 previously described by Jolma *et al*.[38] This process was repeated for four cycles. Ligands
885 were amplified and sequenced after each cycle and before the experiment (the input). When
886 incubating the nucleosome with TF, we initially used 140 mM of monovalent cations. The
887 physiological salt concentration resulted in relatively high nonspecific adsorption of the
888 nucleosome to the sepharose beads. To improve the assay, lower salt concentrations (50 mM
889 to 75 mM) were used in subsequent experiments. Most effects were robust to the changes in
890 the salt concentration; discussion in the main text is limited to observations that were detected
891 under multiple salt concentrations. Moreover, in SELEX, each cycle is essentially an
892 independent replicate of the experiment. The reported effects all show enrichment across
893 multiple SELEX cycles.

894 To interrogate whether the binding of TFs facilitates the dissociation of nucleosome,
895 we carried out a fifth cycle that further separated the TF-bound species into libraries unbound
896 and bound by nucleosome. The TF-bound species were depleted for the nucleosome-bound
897 species with affinity beads for the tag on the histone. The ligands bound by the beads were
898 collected as the nucleosome-bound libraries. The DNA ligands remaining in the supernatant
899 were sequenced as the unbound libraries. As a control, the cycle five nucleosome was also
900 allowed to dissociate in the absence of TFs; the bound library and the unbound library were
901 collected as described above.

902 As a control, HT-SELEX (SELEX using free DNA) with lig147 or with lig200 was
903 performed according to the previous protocol[54,55] with the same purified TF proteins as those
904 used in NCAP-SELEX.

905 The input amount of DNA will exhaust almost all possible 20-bp consecutive or
906 gapped subsequences. Such complexity well suffices the specificity studies of human TFs,
907 whose binding is associated with ~15 bits of infomation on average[55]. For nucleosome, the
908 complexity allows the study of optimal sequences around each histone-DNA contact, but
909 might not capture all the specificities as the nucleosome-favored or disfavored sequences may
910 include cooperation spanning a large length of DNA, e.g., the phased successive bending or
911 the rigidity of a long segment.

912 The NCAP-SELEX and HT-SELEX library for each TF contains hundreds of
913 thousands of unique reads. Under this sample size, if a TF is binding nucleosomal DNA
914 without restrictions, any non-random pattern of TF binding that has a biologically meaningful
915 effect size (as observed in our study) can only occur with an extremely small p-value.

916 **Sequencing and pre-processing**

917 The SELEX ligands amplified with multiplexing primers were purified with AMPure
918 beads (Beckman Coulter), and sequenced using Illumina Hiseq 2000 or Hiseq 4000, with >80

919 bp paired-end settings. Raw sequences were demultiplexed with bcl2fastq (v2.16.0.10). In
920 general hundreds of thousands of reads were obtained for each TF.

921 The R1 and R2 reads of paired-end sequencing were merged with PEAR[84] requiring 5
922 bp overlap at minimum. The merged sequences were discarded if their variable region length
923 is not the same as the ligand design. The obtained sequences were then trimmed for adaptor
924 and for quality by Trim Galore (version 0.4.3). All shorter sequences produced during
925 trimming were removed. The sequences were further cleaned for adaptor sequences by
926 removing all sequences that contained a 14-bp overlap with Illumina sequences. For further
927 analysis, we removed the PCR duplicates and used only the unique reads.

928 **TF signal analysis with E-MI**

929 MI between the most enriched 3-mer pairs (E-MI) was calculated for all non-
930 overlapping position combinations:

931 $$E\text{-}MI(pos1, pos2) = \sum_{top\ \ 3+3\text{-}mers} P(3+3\text{-}mer)\log_2 \frac{P(3+3\text{-}mer)}{P_{pos1}(3\text{-}mer)P_{pos2}(3\text{-}mer)}$$

932 where *P(3+3-mer)* is the observed probability of a 3-mer pair (i.e. gapped or ungapped 6
933 mer) from position 1 and position 2. $P_{pos1}(3\text{-}mer)$ and $P_{pos2}(3\text{-}mer)$, respectively, are the
934 marginal probabilities of the constitutive 3-mers at position 1 and position 2. Their product
935 represents the expected probability of the 3-mer pair. Sums are over the top 10 most enriched
936 3-mer pairs, which have the highest ratio between the observed probability and the expected
937 probability. For the diagonal plot, E-MIs from position pairs where *pos2* = 3 + *pos1* were
938 used.

939 Clustering of the E-MI diagonal was performed using the cosine distance metric and
940 ward.D2 linkage of the *hclust* function in R. The circular representation of the classification
941 result was generated using the *circlize* R package[85]. To calculate the penetration of E-MI for
942 each TF, the diagonal of E-MI was first LOESS smoothed with a span of 0.45; next, for each
943 half of the diagonal, the maximum E-MI value among the half was identified; after that, the
944 positions where the E-MI decreases to half of the E-MI maximum were taken as the
945 penetration depth. The final penetration depth is the average value for both halves of the E-
946 MI diagonal.

947 To check whether the gyre-spanning mode of TF T is preferring nucleosomal DNA,
948 for both its bound and unbound libraries of cycle 5, the E-MI strength of Mode 2 binding was
949 evaluated by summing E-MI from 3-mer pairs spaced 77–83 bp, the E-MI strength of the
950 background was evaluated by summing E-MI from 3-mer pairs spaced 50–70 bp. For both
951 the binding signal and the background, Log2 ratios of E-MI strength between the bound and
952 unbound libraries were calculated for four independent replicates of NCAP-SELEX using TF
953 T. The obtained ratio indicates whether the signal (or the background) has a different strength
954 between the two libraries.

955 When comparing E-MI between the bound and the unbound libraries from cycle five,
956 only TFs with the 3×FLAG tag were considered.

957 **Motif matching and PWM (positional weight matrix) generation**

958 Motif matching for each TF was conducted using MOODS[86,87] with p-value set to
959 0.0001. The motifs used in matching were from our previous curations[54,55]. Motif hits from
960 both strands were combined unless indicated. When necessary, motifs from NCAP-SELEX
961 were generated using Autoseed[38,88] with multinomial of 1.

962 **Quality control of the SELEX experiments**

963 The successful TFs were called by manually checking the E-MI and motif discovery
964 results for each TF. The successful TFs has detectably stronger E-MI between neighboring 3-
965 mer pairs than that between 3-mer pairs far away from each other, and show enriched motifs
966 that are not contaminations from unrelated TFs.

967 **Evaluation of nucleosome-induced orientational preference of TFs**

968 On free DNA, motifs have the same affinity for TF-binding irrespective of its
969 orientation. This is not true when DNA is wrapped onto a nucleosome as the nucleosome
970 breaks DNA's 2-fold rotational symmetry. Depending on motif's relative orientation to
971 nucleosome, the same motifs can differ in affinity. This orientational asymmetry was
972 examined systematically using the lig200 NCAP-SELEX libraries. For each TF, we first
973 calculated the binding energy difference ($\Delta\Delta G$) between the two relative orientations for each
974 of the most enriched non-palindromic 8-mers (top 40 used). The ligands in this TF's SELEX
975 library were divided into two halves according to the dyad position. The two halves were
976 calculated separately and then averaged. Similarly to previous studies[89,90], we assumed a low
977 TF concentration and that the dissociation during wash is insignificant for high-affinity 8-
978 mers. Consequently, for each 8-mer and for each half of the ligands, the $\Delta\Delta G$ of the 8-mer
979 between the two relative orientations is

980 $$\Delta\Delta G = -RTln(\frac{C^r_{5'}/C^r_{3'}}{C^0_{5'}/C^0_{3'}})^{\frac{1}{r}}$$

981 Here $C_{5'}$ and $C_{3'}$ are counts of this 8-mer, respectively for the DNA-strands with their free
982 ends located at the 5' and the 3' (the other end is at the dyad where we divide). The count
983 ratio $C_{5'}/C_{3'}$ in cycle r was normalized with the count ratio in cycle 0, taken the rth root to
984 account for the exponential enrichment in SELEX, and subsequently converted into energy
985 difference. The directional energy difference for each 8-mer was then averaged for the two
986 halves of the ligands, and the absolute value is used to represent the orientational asymmetry
987 of this 8-mer

988 $$Orientation\ asymmetry = abs(\frac{1}{2}\sum_{halves}\Delta\Delta G)$$

989 Orientational asymmetry of the TF is then represented by the mean of the 40 most enriched 8-
990 mers' orientation asymmetry.

991 To rule out any potential orientational bias induced by the adaptors of the SELEX
992 ligands, we also calculated the orientation asymmetry values for 8-mers in the HT-SELEX
993 library. For each TF, the 8-mers used for its HT-SELEX library are the same 8-mers as used

994 for its NCAP-SELEX library. After obtaining the 8-mers' orientation asymmetry values for
995 both the NCAP-SELEX library and the HT-SELEX library of the TF, we used a one-tailed t-
996 test to examine if the orientation asymmetry values in the NCAP-SELEX library are larger
997 than those in the same TF's HT-SELEX library, and obtained the p-value.

998 Signal enrichment in each TF's library was represented using the median fold change
999 of the 8-mers that are most enriched (top 10 8-mers). The fold change for each 8-mer was
1000 calculated using $\log_2$(cycle 4 count / cycle 0 count).

1001 **MNase-seq**

1002 In MNase-seq, the LoVo cell line from ATCC was used (CCL-229, tested to be free
1003 of mycoplasma infection by Hoechst staining). MNase-seq was performed similarly as
1004 described previously[91]. Specifically, 10^7 cells were harvested and washed twice with 10 ml
1005 cold DPBS (Dulbecco's phosphate-buffered saline), spinned down with 350 g for 5 min at 4
1006 °C. The cells were next crosslinked with 10 ml of 1.1% formaldehyde for 10 min in DPBS,
1007 tumbling end over end. The crosslinking reaction was quenched with 50 µl 2.5 M glycine and
1008 further tumbled for 2 min, and washed twice with cold DPBS. Lysis of the cells was
1009 performed with 20 ml 0.5× PBS containing 0.5% Triton X-100 for 3 min on ice; the nuclei
1010 were then collected by centrifugation (350 g, 5 min). Before MNase digestion, the nuclei
1011 were washed three times with 1× MNase digestion buffer, resuspended with 1 ml of the same
1012 buffer containing 100 µg/ml RNase A. An aliquot of 100 µl was used for MNase digestion.
1013 MNase digestion was carried out with 100 units of MNase (M0247S, NEB) at 37 °C for 8
1014 min, quenched with 100 µl stop buffer (40 mM EDTA, 40 mM EGTA, 1% SDS, 1.5 mg/ml
1015 proteinase K) at 65 °C o/n. The MNase fragments with length of 100–1000 bp were selected
1016 using Ampure beads (Beckman Coulter), and subjected to the library preparation workflow of
1017 Illumina (E7370L, NEB). The paired-end sequencing (2 × 86 bp) was performed using
1018 Illumina HiSeq 4000.

1019 MNase-sequencing data from K562 cell line were downloaded from GEO accession
1020 GSE78984. Three titration series (20.6U, 79.2U and 304U) of MNase were selected.

1021

1022 **Combined analysis of MNase-seq and ChIP-seq**

1023 For MNase-seq data, the raw sequencing reads were quality and adapter trimmed with
1024 cutadapt version 1.12 in Trim Galore (version 0.4.3). Low-quality ends trimming was done
1025 using Phred score cutoff 30. Adapter trimming was performed using the first 13 bp of the
1026 standard Illumina paired-end adapters with default parameters. Raw sequencing reads were
1027 mapped to the human reference genome (hg19) using bwa[92] with default parameters.
1028 Duplicates were removed with samtools (v 1.3.1) rmdup function. Insert size distribution was
1029 calculated based on 10000 reads that were aligned to autosomes. After duplicate removal,
1030 data from K562 titration series were merged.

1031 Coverage of MNase fragments with length >140bp was calculated at ChIP-seq peaks
1032 of 20 TFs in K562 cell lines. We selected 500 highest signal ChIP-seq peaks that had
1033 respective TF's motif match site and did not overlap with hg19 blacklist genomic regions.

1034 BEDtools (v2.26.0) genomecov and intersect functions were utilized in calculations.
1035 ENCODE narrowPeak calls including two replicates were used from March 2012 freeze
1036 (UCSC wgEncodeAwgTfbsUniform track) release for ATF3, CEBPB, CTCF, ELF1,
1037 GATA2, JUND, SRF, USF2 and YY1, and from later releases (the ENCODE Portal
1038 http://www.encodeproject.org, accessed 07/12/2017) for ATF2, CREB3L1, CREM, ELF4,
1039 HMBOX1, MYBL2, NFATC3, PKNOX1, RFX1, SREBF1 and YBX1[72]. Genomic sites
1040 recognized by each motif retrieved from previous HT-SELEX runs were searched from the
1041 human genome using program MOODS[86] with a p-value cut-off of 10^{-4} and a score cut-off of
1042 5. Final MNase fragment coverage values were calculated by taking the average of multiple
1043 motifs for each TF, and correlated with E-MI penetration values with Pearson's method.

1044 V-plots were generated as described by Henikoff *et al.*[45]. MNase-fragments aligned to
1045 autosomes were used. The LoVo ChIP-seq data from Yan et al.[37] were downloaded from
1046 GEO accession GSM1239499 and GSM1208610. The peak calls were transformed from
1047 hg18 to hg19 coordinates by using UCSC liftOver and peaks within hg19 blacklist genomic
1048 regions were excluded. Genomic sites recognized by each motif were searched from the
1049 human genome using MOODS[86] with a p-value cut-off of 10^{-4} and a score cut-off of 5.
1050 Center-point coordinates of MNase-fragments and motif sites within ChIP-peaks were
1051 compared using BEDtools (v2.26.0) closest function using strand information of each motif
1052 match.

1053 **Fast Fourier Transformation (FFT) analysis and structure alignment**

1054 The diagonal of E-MI for each TF's library was subtracted with the mean, windowed
1055 by Welch's function, and then subjected to FFT. The obtained power spectrum was further
1056 divided with the mean of the E-MI diagonal and the length of the diagonal. We next
1057 calculated FFT-AUC (area under the curve) from the power spectrum and used it as an
1058 indicator for the ~10 bp periodicity induced by nucleosome. The FFT-AUC was calculated
1059 for frequencies ranging from 0.08–0.12 bp^{-1} and subtracted with the baseline level (estimated
1060 from 0.14–0.3 bp^{-1}). The phase of FFT was examined at 0.102 bp^{-1}. The same process was
1061 applied to the TA dinucleotide counts across all positions of the ligand for the NCAP-SELEX
1062 library of all individual TFs.

1063 To mimic the in-phase and out-of-phase bindings of the periodic binders with respect
1064 to the preferred TA positions on nucleosome, the available structure of TF-DNA complex
1065 was aligned to the nucleosome by matching the center of the TF's core binding sequence
1066 either to the TA step (in phase), or to a step 5-bp downstream of the TA step (out of phase).
1067 The 6-bp core binding sequence in the structure of TF-DNA complex is defined according to
1068 the most enriched 6-mers in this TF's NCAP-SELEX library. To make the alignment, C1–C4
1069 on all deoxyribose rings were matched between the 6-bp core binding sequence and the 6-bp
1070 nucleosomal DNA centered in-phase or out-of-phase to the TA step.

1071 **Electrophoretic mobility shift assay (EMSA)**

1072 Nucleosomes were formed essentially as described previously[39] from the histone
1073 octamers and the modified Widom 601[93] DNA sequence

CTGGAGAATCCCGGTCTGCAGGCCGCTCAATTGGTCGTAGACAGCTCTAGCACCG CTTAAACGCACGTACGGTATTGTTTATTTTGTTCCTCCGCCAAGGGGATTACTCCC TAGTCTCCAGGCACGTGTCAGATATATACATCCTGT. The modified Widom 601 is embedded with a SOX11-binding segment (GGTATTGTTTATTTTGTTCCT) at the center. The sequence of the embedding segment is extracted from a ligand in the cycle 4 SELEX library of SOX11. The embedding position on Widom 601 is the same as the segment's original position on the SELEX ligand. Nucleosomes were reconstituted using this modified Widom 601 ligand and subsequently heat-shifted at 55°C for 30 min. Next the nucleosomes (containing 1 µg DNA) were incubated on ice with purified SOX11 eDBD in a 40 µl volume. As a control, the SOX11 eDBD were also directly incubated with 1 µg modified Widom 601 ligand in 40 µl volume. The samples were then subjected to EMSA. A 0.8% agarose gel was cast and run in the 0.2x Tris–Boric acid–EDTA (TBE) buffer. EMSA was performed in native conditions at 4°C for 1 h at 120 V, and later the gel was post-stained in DNA Stain Clear G (Serva). The DNA ladder 100 bp (NEB) was used as the marker.

84 Zhang, J. J., Kobert, K., Flouri, T. & Stamatakis, A. PEAR: a fast and accurate Illumina Paired-End reAd mergeR. *Bioinformatics* **30**, 614-620 (2014).

85 Gu, Z., Gu, L., Eils, R., Schlesner, M. & Brors, B. *circlize* Implements and enhances circular visualization in R. *Bioinformatics* **30**, 2811-2812 (2014).

86 Korhonen, J., Martinmaki, P., Pizzi, C., Rastas, P. & Ukkonen, E. MOODS: fast search for position weight matrix matches in DNA sequences. *Bioinformatics* **25**, 3181-3182 (2009).

87 Pizzi, C., Rastas, P. & Ukkonen, E. Finding significant matches of position weight matrices in linear time. *IEEE/ACM Trans. Comput. Biol. Bioinform.* **8**, 69-79 (2011).

88 Nitta, K. R. *et al.* Conservation of transcription factor binding specificities across 600 million years of bilateria evolution. *Elife* **4**, e04837 (2015).

89 Slattery, M. *et al.* Cofactor binding evokes latent differences in DNA binding specificity between Hox proteins. *Cell* **147**, 1270-1282 (2011).

90 Riley, T. R. *et al.* SELEX-seq: a method for characterizing the complete repertoire of binding site preferences for transcription factor complexes. *Methods Mol. Biol.* **1196**, 255-278 (2014).

91 Mieczkowski, J. *et al.* MNase titration reveals differences between nucleosome occupancy and chromatin accessibility. *Nat. Commun.* **7**, 11485 (2016).

92 Li, H. & Durbin, R. Fast and accurate short read alignment with Burrows-Wheeler transform. *Bioinformatics* **25**, 1754-1760 (2009).

93 Lowary, P. T. & Widom, J. New DNA sequence rules for high affinity binding to histone octamer and sequence-directed nucleosome positioning. *J. Mol. Biol.* **276**, 19-42 (1998).

94 Collings, C. K., Fernandez, A. G., Pitschka, C. G., Hawkins, T. B. & Anderson, J. N. Oligonucleotide sequence motifs as nucleosome positioning signals. *PLoS ONE* **5**, e10933 (2010).

95 Jolma, A. *et al.* Multiplexed massively parallel SELEX for characterization of human transcription factor binding specificities. *Genome Res.* **20**, 861-873 (2010).

1113 **EXTENDED DATA FIGURES**

Extended Data Figure 1, Zhu et al. 2017

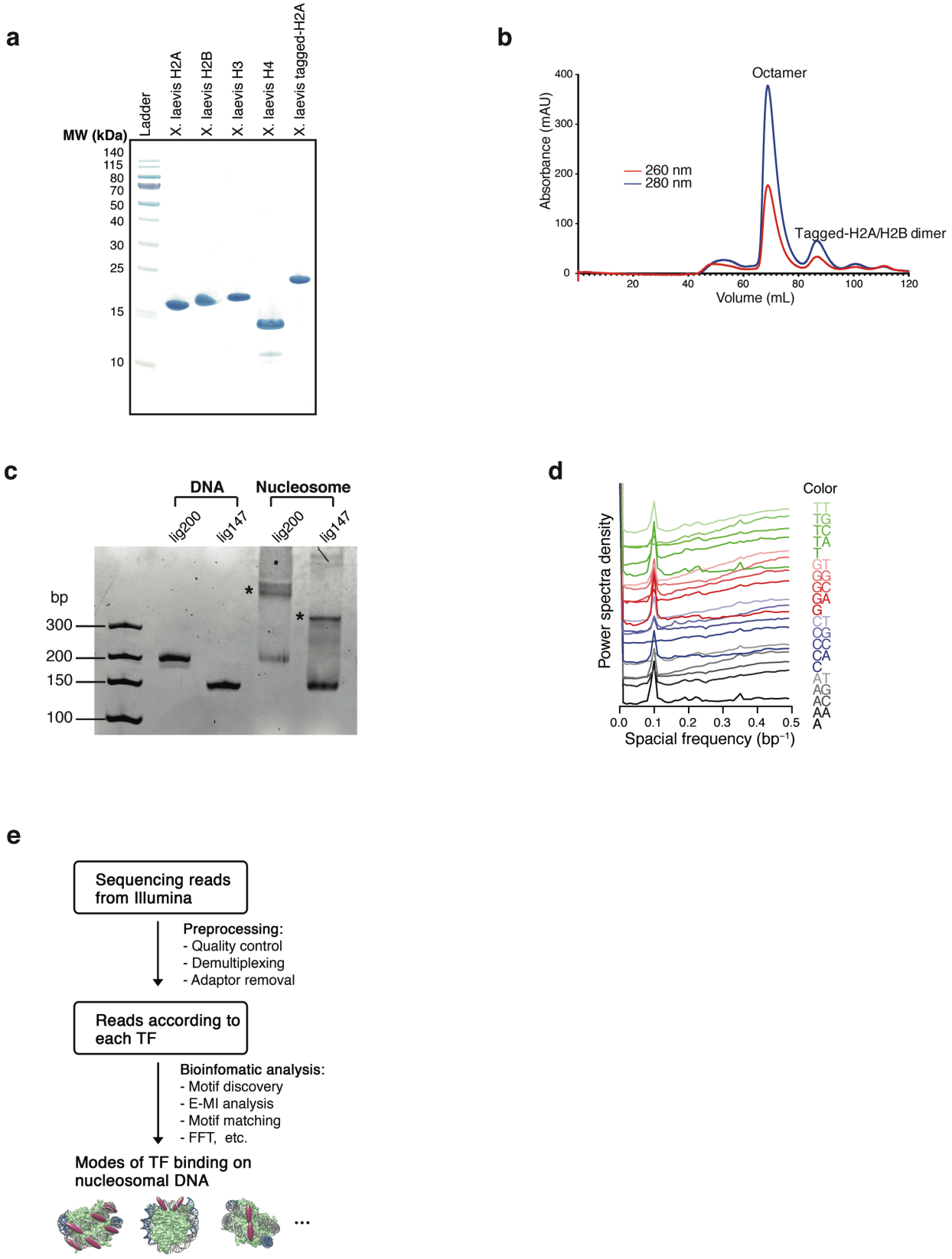

1114

1115 **Extended Data Figure 1 | Quality control and analysis pipeline. a,** Expression of the
1116 recombinant histones from *X. laevis*. For each lane 3 μg histone is loaded. **b,** Size-exclusion
1117 chromatogram of the histone octamer. **c,** EMSA result showing the reconstituted
1118 nucleosomes using lig147 and lig200. The original ligands are also loaded as reference. The
1119 asterisks indicate the nucleosome bands. **d,** Oligonucleotide periodicity in the library
1120 enriched by nucleosome. As a quality control of nucleosome reconstitution, we verified
1121 whether nucleosome by itself is enriching the previously reported ~10-bp periodic
1122 oligonucleotide signal[93,94]. Nucleosome SELEX (without TF) were carried out for four cycles
1123 to enrich nucleosome-favoring ligands. The counts of each single and di-nucleotide across
1124 each individual ligand were Fourier transformed and summed up for the whole library. A
1125 clear peak around 0.1 bp^{-1} (corresponding to the reported ~10-bp periodicity) is visible for
1126 most mono and dinucleotides. **e,** Analysis pipeline for the ligands enriched in NCAP-SELEX.
1127

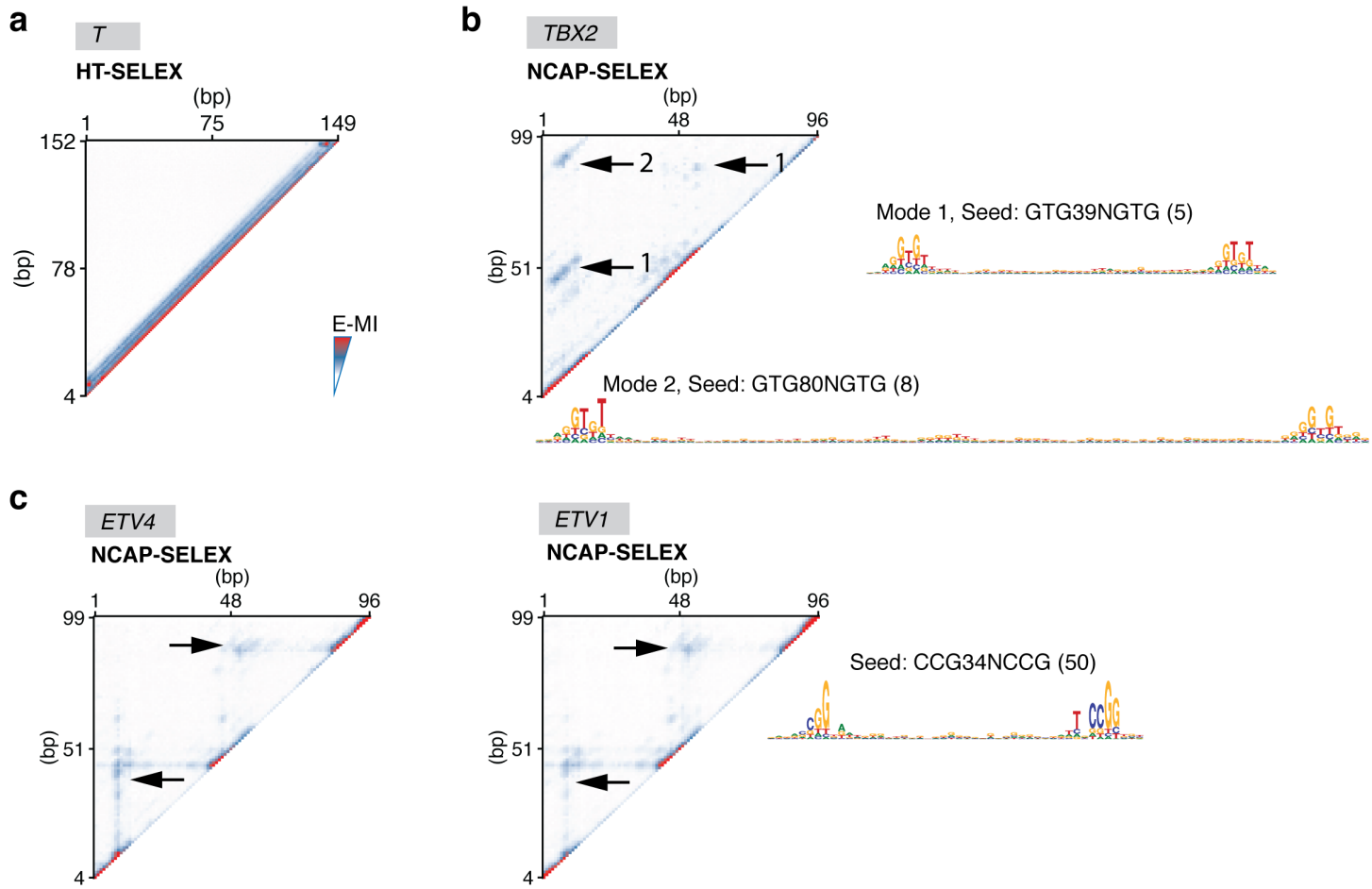

Extended Data Figure 2 | Specific binding modes allowed on nucleosome. a, E-MI heatmap of T (brachyury) in HT-SELEX using lig200. Pairwise E-MI for all 3-mer pairs is presented as a heatmap. The signal is only visible near the diagonal, no E-MI signal across ~80 bp is detected. **b,** E-MI heatmap of TBX2 in NCAP-SELEX using lig147. The E-MI signals across ~80 (mode 1) and ~40 bp (mode 2) are indicated. The corresponding motif of each mode is derived with the indicated seed for a specific position (number in the parentheses) in the high E-MI regions. PWM generation follows our previous method[95] using multinomial 1. **c,** E-MI heatmap of ETV4 and ETV1 in NCAP-SELEX using lig147. The E-MI signal across ~40 bp is indicated. The motif is derived as in (**b**).

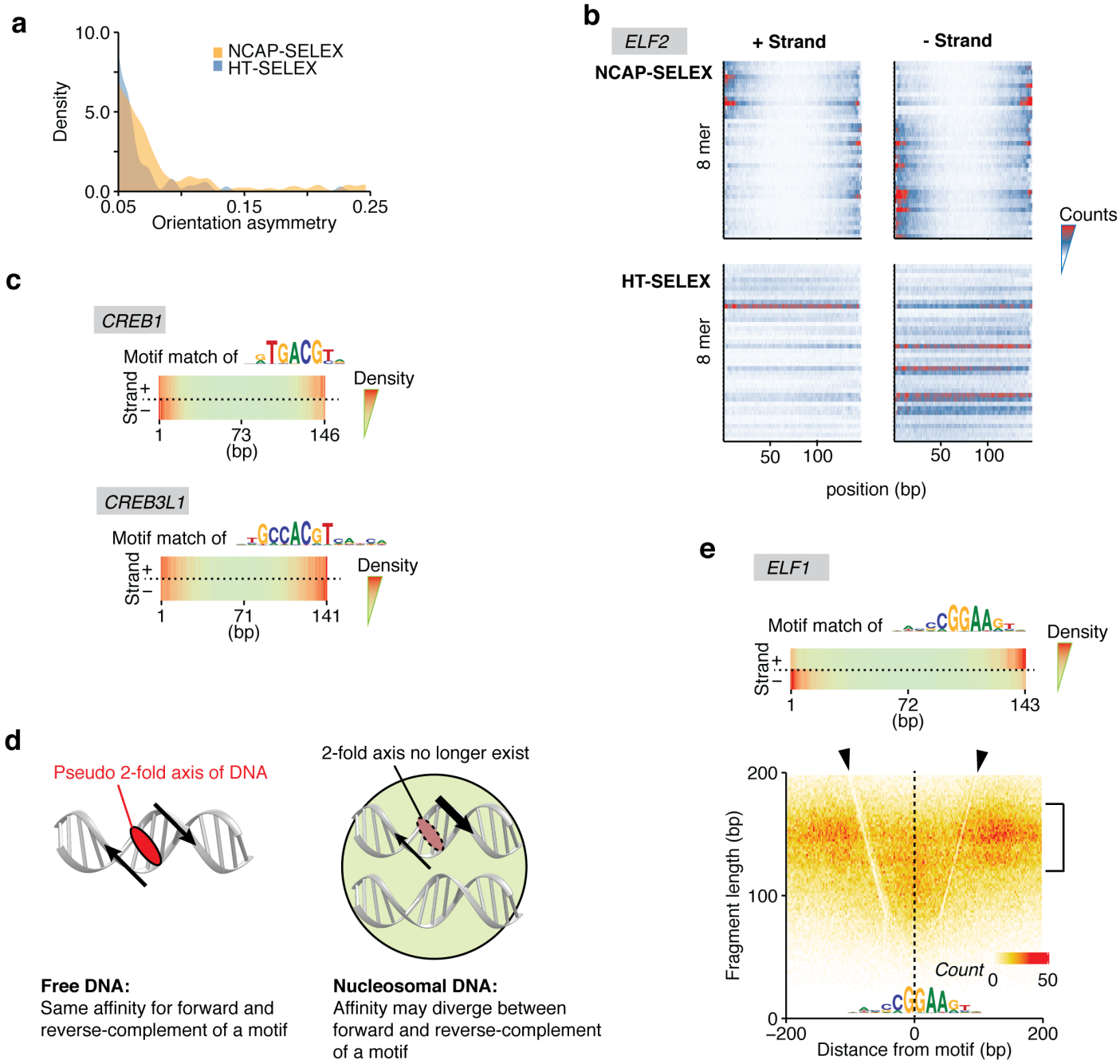

Extended Data Figure 3 | Nucleosome breaks the rotational symmetry of DNA. a, Density plot representing the orientation asymmetry of all TFs in NCAP-SELEX and in HT-SELEX. In NCAP-SELEX, more TFs bind with high orientational asymmetry than in HT-SELEX. A few TFs can prefer different ends of the ligand for the two binding directions in HT-SELEX; this is likely induced by the adaptor sequences. However, there are more TFs with higher orientational asymmetry in NCAP-SELEX libraries, despite the fact that for most TFs their signals are stronger in HT-SELEX libraries. **b,** Orientation asymmetry of ELF2 revealed by using top 8-mers. Each row of the heatmap corresponds to the counts distribution of a top 8-mer (non-palindromic) across the positions of the SELEX ligand. Hits of the top 8-mers occur at different ends for different strands of nucleosomal DNA (i.e. an 8-mer and its

1150 reverse-complement prefer different ends), whereas their distribution is relatively
1151 homogeneous for free DNA. **c,** Orientation asymmetry of CREB TFs. CREB TFs have
1152 different motif density distributions for the two strands of nucleosomal DNA. The motif used
1153 for matching is indicated above. The "–" strand profile is from the density of the reverse-
1154 complement motif. **d,** Break of the 2-fold rotational symmetry of DNA induces preferred
1155 orientation of TFs. Left: free DNA has a 2-fold axis (red ellipse) perpendicular to the helix
1156 axis. Motifs in two orientations are symmetric with each other with respect to a 180° rotation
1157 centered on the axis. Right: for motifs on nucleosomal DNA, if the other strand of DNA or
1158 the histone proteins (green) affects binding, the 2-fold axis of DNA no longer exists, as a
1159 180° rotation centered on the axis no longer generates an identical conformation (the rotated
1160 image not superimposable with the original one). **e,** Orientational asymmetry of ELF1 on
1161 nucleosomal DNA. Similar to ELF2, ELF1 has different motif density distributions for the 2
1162 strands of nucleosomal DNA (top panel). The distribution of MNase fragments around
1163 genomic ELF1 sites is also asymmetric (bottom panel); footprint of ELF1 is indicated with
1164 the arrowheads (the V-shaped lines with a lower signal density), and the range of flagment
1165 length that corresponds to nucleosome occupasion are indicated with the bracket.
1166

Extended Data Figure 4, Zhu et al. 2017

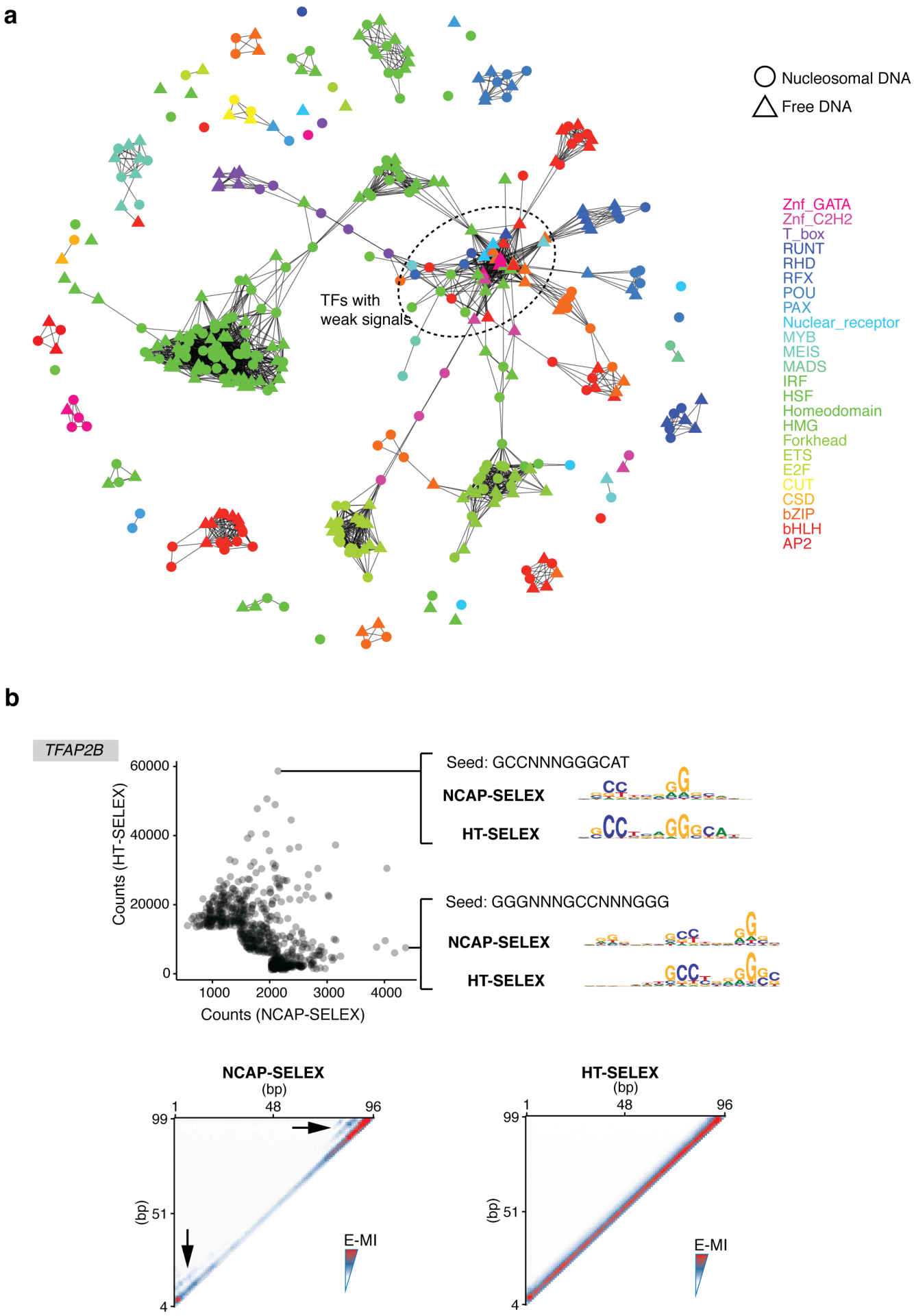

1168 **Extended Data Figure 4 | Most TFs bind nucleosomal DNA without significant motif**
1169 **change. a,** Network representation of TFs' specificities in presence and absence of the
1170 nucleosome. Vertices indicate the binding specificity profiles of TF eDBDs, either in the
1171 presence (circle) and in the absence (triangle) of the nucleosome. Vertices are colored
1172 according to the TF's family. Two vertices are connected by an edge if the profiles they
1173 represent are similar. Specifically, we assume that all 9-mer counts in the library enriched by
1174 a TF will serve as a profile to represent its binding specificity. To evaluate the similarity
1175 between two profiles, we selected the most abundant 9-mers (top 0.1%) from either of the
1176 profiles, and calculated Pearson's correlation using counts of these 9-mers from both of the
1177 two profiles. An edge is drawn between the profiles (vertices) if the calculated correlation is
1178 greater than 0.2. TFs from the same family generally clusters together regardless of the
1179 presence of nucleosome, indicating that TFs' binding specificity is not significantly affected
1180 by nucleosome. TF profiles with weak signals also tend to cluster together (the cluster circled
1181 by dashed line), as the top 9-mers in their libraries are dominated by SELEX bias (e.g. the
1182 bias from PCR or wash) rather than by the TFs' specificities. **b,** TFAP binds nucleosomal
1183 DNA with slightly different specificity than free DNA. The scatter plot (top panel) shows the
1184 counts of gapped 9-mers from SELEX libraries of TFAP2B, enriched with NCAP-SELEX (x
1185 axis) and HT-SELEX (y axis). The examined 9-mers consists of three segments of trimers
1186 interspaced with two gaps (0–5 bp). Only the most enriched 9-mers (top 300 in each library
1187 and in the combined library) are shown from clarity. For comparison, the most differentially
1188 enriched gapped 9-mers were also used as seeds to derive the corresponding motifs from both
1189 libraries (right). The heatmap (bottom panel) shows the pairwise E-MI for all combinations of
1190 positions on lig147, in the presence (left) and absence (right) of nucleosome. The arrowheads
1191 indicate the additional signals developed in the presence of nucleosome.
1192

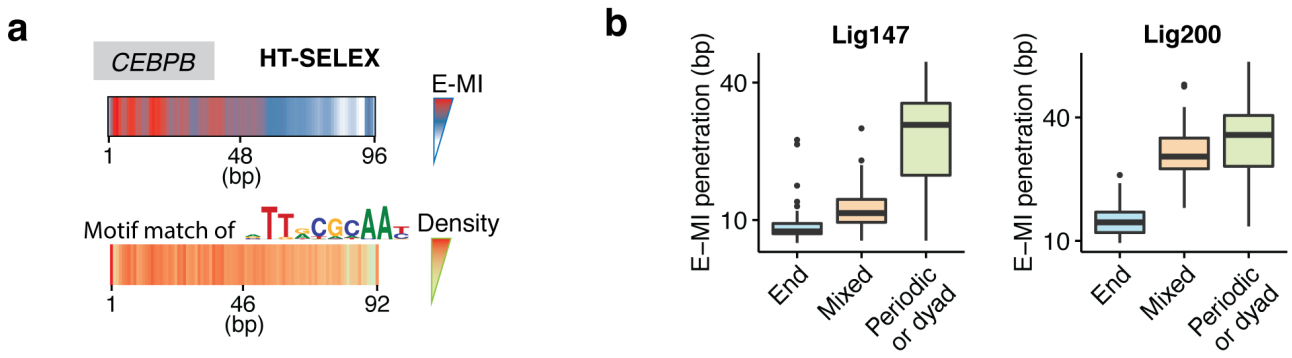

Extended Data Figure 5 | Control experiment for the end-binders and E-MI penetration according to binder classes. a, E-MI diagonal and motif matching results for the bZIP factor CEBPB in HT-SELEX. Without nucleosome, its signal distributes relatively homogeneously across the ligand. **b,** Penetration of E-MI signal for each binder class of TFs on lig147 and lig200. The results with SELEX ligands of different lengths generally correspond with each other. The periodic/dyad binders show deeper E-MI penetration than the end binders and thus are more capable of binding nucleosomal DNA. The boxes indicate the middle quartiles, separated by median line. Whiskers indicate last values within 1.5 times the interquartile range for the box.

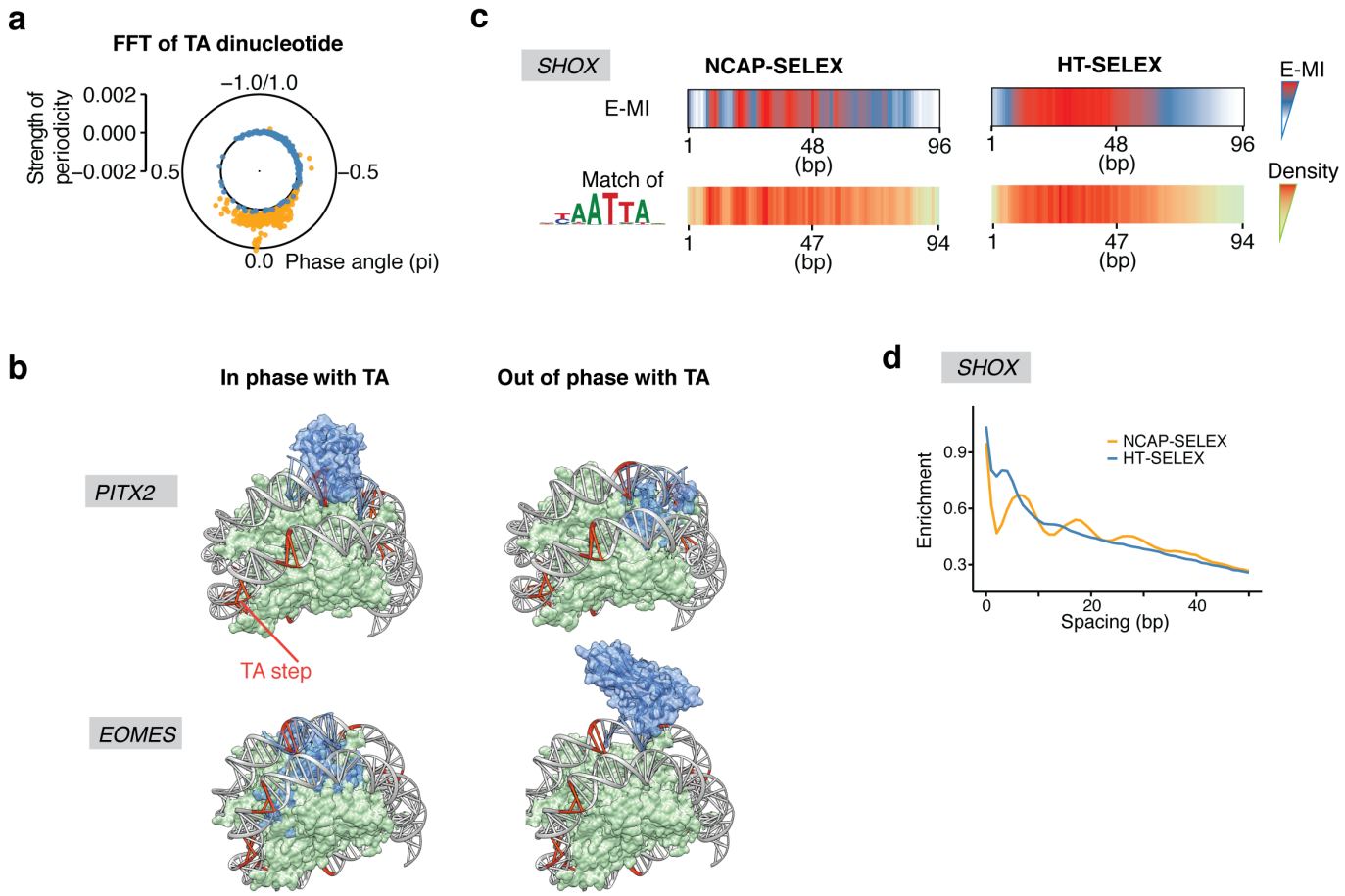

Extended Data Figure 6 | Analysis of the periodic binders. a, Strength and phase of the ~10 bp periodicity of TA dinucleotide in NCAP-SELEX and HT-SELEX libraries. For the library (lig147) enriched by a specific TF, the strength and phase information is derived from FFT of the TA counts at each position of the library. In the polar plot, each dot represents one TF's library. The overall periodicity is stronger in the NCAP-SELEX libraries (yellow) than in the HT-SELEX libraries (blue), suggesting an enrichment of nucleosome signal. The TA phases in all TFs' NCAP-SELEX libraries are similar, thus the rotational positioning of nucleosome on the SELEX ligand is similar for all TF's libraries. **b,** Cartoon representations of the 3D structures of PITX3 (PDB 2lkx) and TBX5 (T_box, PDB 2x6v) in complexes with nucleosomal DNA. The DNA ligand in the nucleosome structure (PDB 3ut9) contains phased TA steps (orange). Consistent with the SELEX result, PITX is more compatible with nucleosomal DNA when it binds in phase with TA, whereas T-box is more compatible when it binds out of phase with TA. **c,** E-MI diagonal and motif matching results for SHOX in NCAP-SELEX and HT-SELEX. **d,** The ~10 bp periodicity for the preferred spacing of SHOX dimers on nucleosomal DNA. In NCAP-SELEX libraries of many periodic binders (SHOX as an example), enrichment of the most abundant 3-mer tandem repeats oscillates as a function of the spacing between the repeats. The enrichment is evaluated by log2-ratio between the observed and expected occurrences.

a

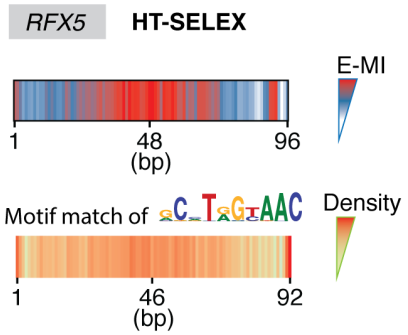

Extended Data Figure 7 | Analysis of the dyad binders. a, E-MI diagonal and motif matching results for RFX5 in HT-SELEX. The distribution of binding events is homogeneous in the absence of nucleosome.

Extended Data Figure 8, Zhu et al. 2017

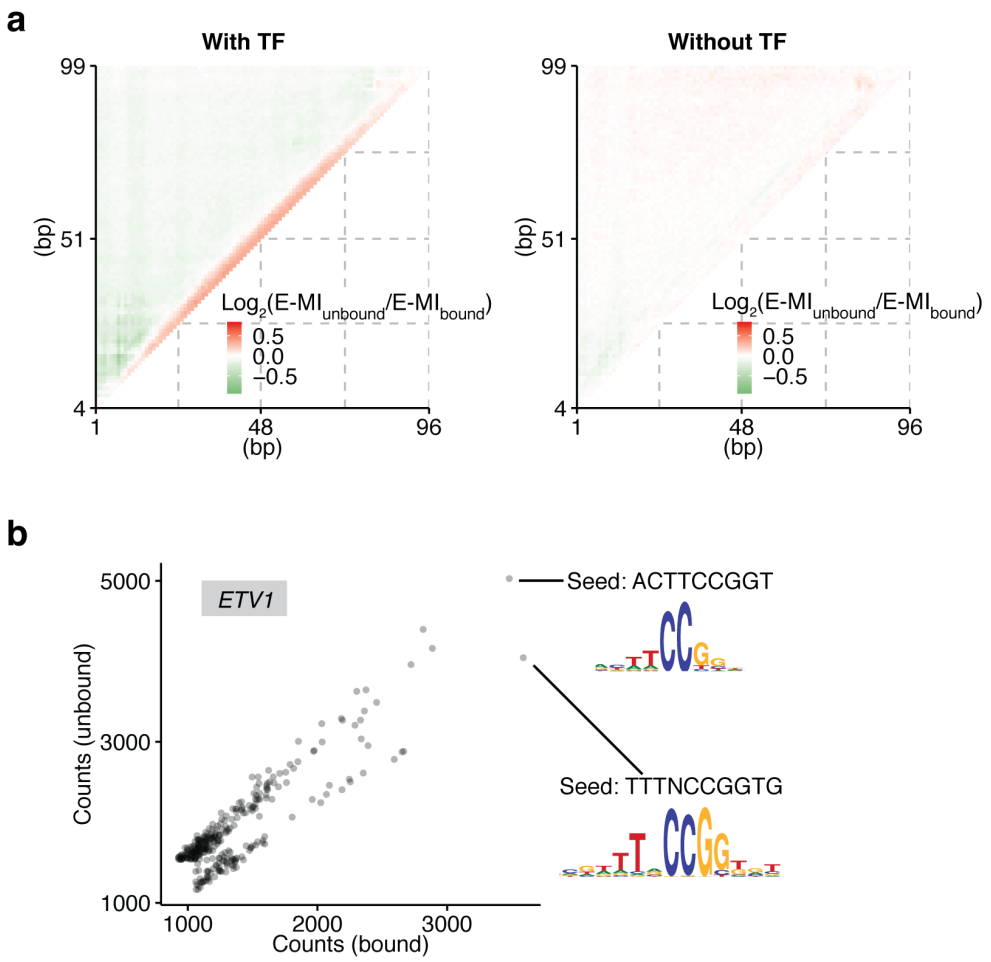

Extended Data Figure 8 | Effects of TF binding on the stability of nucleosome. **a,** E-MI difference between the bound and the unbound cycle 5 libraries. The bound and the unbound libraries were collected either in the presence (left) or in the absence (right) of TFs. The heatmaps visualize E-MI differences between the bound and unbound libraries for all position combinations of 3-mer pairs, and each pixel on the heatmap is a mean of all the examined TFs' E-MI difference at this pixel. For individual TFs, value at each pixel is calculated as $\log_2(E\text{-}MI_{unbound}/E\text{-}MI_{bound})$. Testing nucleosome dissociation in the absence of TF was aimed to verify whether the TF motifs on lig147 by themselves can affect the nucleosome's stability. **b,** The efficiency of nucleosome dissociation induced by ETV1 is dependent on its binding mode. The shorter mode is more efficient than the longer mode in displacing nucleosome, as it enriches more in the dissociated library (unbound).